1 **_b3galt6_ knock-out zebrafish recapitulate β3GalT6-deficiency disorders in**

2 **human and reveal a trisaccharide proteoglycan linkage region**

3 Sarah Delbaere[a], Adelbert De Clercq[a], Shuji Mizumoto[b], Fredrik Noborn[c,d], Jan Willem Bek[a], Lien

4 Alluyn[a], Charlotte Gistelinck[e], Delfien Syx[a], Phil L. Salmon[f], Paul J. Coucke[a], Göran Larson[c,d], Shuhei

5 Yamada[b], Andy Willaert[a,1], Fransiska Malfait[a,1,2]

6 [a]Center for Medical Genetics Ghent, Department of Biomolecular Medicine, Ghent University and

7 Ghent University Hospital, Ghent, Belgium.

8 [b]Department of Pathobiochemistry, Faculty of Pharmacy, Meijo University, 150 Yagotoyama,

9 Tempaku-ku, Nagoya, Aichi 468-8503, Japan.

10 [c]Department of Laboratory Medicine, Sahlgrenska Academy at the University of Gothenburg,

11 Gothenburg, Sweden.

12 [d]Laboratory of Clinical Chemistry, Sahlgrenska University Hospital, Gothenburg, Sweden.

13 [e]Department of Orthopaedics and Sports Medicine, University of Washington, Seattle, WA98195.

14 [f]Bruker microCT, Kontich, Belgium.

15

16 [1]AW and FM contributed equally to this work.

17

18 [2]Corresponding author:

19 Fransiska Malfait

20 Center for Medical Genetics, Ghent University Hospital, 0K5

21 Corneel Heymanslaan 10, B-9000 Ghent, Belgium

22 Tel: +32-9-332 36 03

23 E-mail: Fransiska.Malfait@UGent.be

24

25

26

Keywords

b3galt6, zebrafish, trisaccharide linkage region, proteoglycans, linkeropathies

Author Contributions

SD, AW and FM designed the study; SD, ADC, SM, FN, JWB, LA and CG performed research; SM, PLS, GL, SY contributed new reagents or analytic tools; SD, ADC, SM, FN, JWB, LA, CG, DS, PLS, PJC, GL, SY, AW and FM analyzed data; SD, AW and FM wrote the paper; all authors reviewed the paper.

Abstract

Proteoglycans are structurally and functionally diverse biomacromolecules found abundantly on cell membranes and in the extracellular matrix. They consist of a core protein linked to glycosaminoglycan chains via a tetrasaccharide linkage region. Here, we show that CRISPR/Cas9-mediated *b3galt6* knock-out zebrafish, lacking galactosyltransferase II, which adds the third sugar in the linkage region, largely recapitulate the phenotypic abnormalities seen in human β3GalT6-deficiency disorders. These comprise craniofacial dysmorphism, generalized skeletal dysplasia, skin involvement and indications for muscle hypotonia. In-depth TEM analysis revealed disturbed collagen fibril organization as the most consistent ultrastructural characteristic throughout different affected tissues. Strikingly, despite a strong reduction in glycosaminoglycan content, as demonstrated by anion-exchange HPLC, subsequent LC-MS/MS analysis revealed a small amount of proteoglycans containing a unique linkage region consisting of only three sugars. This implies that formation of glycosaminoglycans with an immature linkage region is possible in a pathogenic context. Our study therefore unveils a novel rescue mechanism for proteoglycan production in the absence of galactosyltransferase II, hereby opening new avenues for therapeutic intervention.

2

Introduction

Proteoglycans (PGs) comprise a group of complex biomacromolecules, consisting of a core protein and one or multiple glycosaminoglycan (GAG) side chains, that are ubiquitously expressed in the extracellular matrix (ECM) and on cell surfaces and basement membranes in vertebrate and invertebrate species [1-4]. Besides their structural role, PGs act as mediators between the ECM and intracellular signaling pathways and contribute to development and tissue homeostasis, influencing a variety of cellular processes including cell fate determination, cell proliferation, migration, adhesion, differentiation and survival [5].

The PG superfamily is, depending on the composition of the GAG chains, subdivided into heparan sulfate (HS) and chondroitin/dermatan sulfate (CS/DS) PGs. These GAG chains are linear polysaccharides, composed of a repeated disaccharide unit consisting of an uronic acid and amino sugar. HSPGs, such as perlecan, syndecan and glypican, consist of repeating glucuronic acid (GlcA)- *N*-acetyl-glucosamine (GlcNAc) disaccharides. CSPGs consist of repeating GlcA- *N*-acetyl-galactosamine (GalNAc) disaccharides. DS is a stereoisomer of CS, in which GlcA is epimerized to iduronic acid (IdoA). In mammalian tissues, CS and DS chains are often present as hybrid CS-DS chains on PGs (e.g. decorin, biglycan) [6]. Tightly controlled modifications, such as epimerization and sulfation reactions, further increase the structural and functional diversity of the HS and CS/DS PGs [7, 8]. GAG biosynthesis of both HSPGs and CS/DSPGs is initiated in the endoplasmic reticulum and Golgi apparatus by the formation of a common tetrasaccharide linkage region (glucuronic acid-galactose-galactose-xylose-*O*--) (GlcA-Gal-Gal-Xyl-*O*-) via *O*-glycosylation of a serine residue of the core protein (Fig. 1A) [1-3]. The first step in the biosynthesis of this tetrasaccharide linkage region is catalyzed by xylosyltransferases (XylTs) encoded by the paralogues *XYLT1* [MIM 608124] and *XYLT2* [MIM 608125] [9]. Two Gal residues are subsequently added by respectively galactosyltransferase I (GalT-I or β4GalT7 encoded by *B4GALT7* [MIM 604327]) and galactosyltransferase II (GalT-II or β3GalT6 encoded by *B3GALT6* [MIM 615291]) [10, 11]. Further addition of a GlcA by glucuronosyltransferase I (GlcAT-I encoded by *B3GAT3)* [MIM 606374] completes the formation of the linkage region [12].

The cellular machinery required for GAG biosynthesis and modification is conserved over a broad range of eukaryotic organisms [13]. The particular importance of a correct initiation of GAG synthesis is underscored by the identification of a series of severe, overlapping and multisystemic genetic human disorders that result from deficient activity of any of these "linkage-enzymes", collectively coined as 'linkeropathies' [14-16]. The most frequently reported linkeropathy results from galactosyltransferase II deficiency, caused by biallelic pathogenic variants in *B3GALT6.* This leads to two clinically overlapping conditions, spondylodysplastic Ehlers-Danlos syndrome (EDS) (spEDS-*B3GALT6*) and

3

88   spondyloepimetaphyseal dysplasia with joint laxity type I (SEMD-JL1) [16, 17], both of which are

89   characterized by variable degrees of spondyloepimetaphyseal bone dysplasia, (with postnatal growth

90   restriction, bowing of long bones, hypo- or dysplasia of iliac and long bones, and vertebral body

91   changes), kyphoscoliosis, bone fragility with spontaneous fractures, joint hypermobility in conjunction

92   with joint contractures, hypotonia with delayed motor development, skin fragility, and craniofacial

93   dysmorphisms, including midfacial hypoplasia and dysplastic teeth [16-18]. The severe and pleiotropic

94   phenotype suggests a critical role for *B3GALT6* in the development and homeostasis of various

95   connective tissues. Pathogenic variants in *B3GALT6* either result in mislocalization and/or reduced

96   amounts of active galactosyltransferase II [19]. Previous studies on several biallelic *B3GALT6* variants

97   showed that they resulted in a barely detectable *in vitro* galactosyltransferase II enzymatic activity, but

98   intriguingly HS and CS/DS GAG synthesis was partially preserved *in cellulo* [20]. While some variants

99   may have a greater deleterious effect on the *in vitro* than on the *in cellulo* enzymatic activity, it is

100 currently unknown whether there are rescue mechanisms at play to (partially) compensate for the

101 galactosyltransferase II activity.

102 In recent years, zebrafish have emerged as an excellent tool to model disease and to increase our

103 understanding of developmental processes and disease mechanisms. Zebrafish share 70% of their

104 genes with humans [21] and the advantages of their use are reflected by their large breed size, short

105 lifecycle and low husbandry costs [22]. Zebrafish has proven to be a relevant genetic model for the

106 study of PG biosynthesis since many enzymes involved in this process are strongly conserved between

107 human and zebrafish [23], and a number of zebrafish models for defective PG synthesis (including

108 *fam20b^{b1125}, xylt1^{b1189}, or b3gat3^{hi307}*), provided novel knowledge on PG function in bone and cartilage
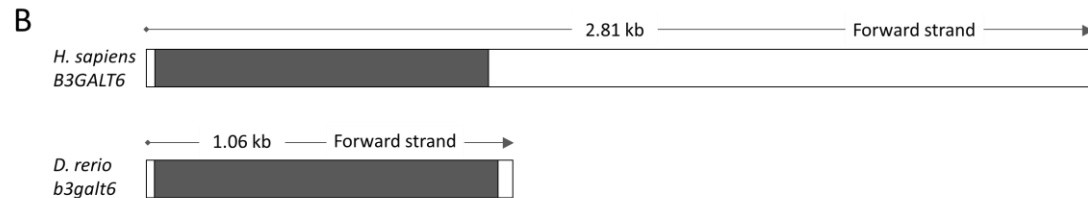
109 formation [23-26].

110 In this study, we generated *b3galt6* knock-out (KO) zebrafish as a model for spEDS-*B3GALT6* and SEMD-

111 JL1. These models were used to investigate the structure and amount of different GAG disaccharides

112 and the PG linkage region composition in these disorders. Furthermore, in-depth phenotypic

113 characterization of *b3galt6^{-/-}* zebrafish was done to reveal to which extent key features of the human

114 disorders are recapitulated and to further elucidate the function of galactosyltransferase II in

115 vertebrate musculoskeletal development.

116

117

118

119

4

Results

CRISPR/Cas9-mediated *b3galt6* knock-out in zebrafish leads to reduced HS and CS/DS glycosaminoglycan concentrations in bone, muscle and skin

Similar to its human orthologue, zebrafish *b3galt6* (NM_001045225.1) is a single-exon gene (Fig. 1B). Human and zebrafish galactosyltransferase II (β3GalT6/B3galt6) protein sequence display 82.5 % amino acid (AA) similarity, with the highest AA conservation in the luminal domain (Fig. 1C).

In order to investigate the consequences of zebrafish B3galt6-deficiency on GAG biosynthesis in different tissues, we generated two *b3galt6* KO zebrafish models using CRISPR/Cas9 gene editing. The first KO model carries the c.181delinsAAAGAGCTCCTAAAGGG indel mutation (cmg20 allele), leading to a premature termination codon (PTC) (p.(Phe68*)), located upstream to the catalytic domain (Fig. 1D). RT-qPCR showed a 40.3% reduction of *b3galt6 mRNA* expression in homozygous adult *b3galt6* KO zebrafish compared to wild-type (WT) siblings (Fig. 1E). For the remainder of this manuscript, this model will be referred to as *b3galt6*$^{-/-}$. The second KO model carries a four base pair deletion (c.398_401del) (cmg22 allele), predicted to generate a PTC (p.(Asn139*)) in the catalytic domain (NM_001045225.1). This mutant was solely used for validation purposes (Fig. S1). Both *b3galt6* KO zebrafish were produced at an expected Mendelian ratio and survived into adulthood. Unfortunately, commercial antibodies, which were only available against human β3GalT6, did not work in our hands and precluded the investigation of zebrafish B3galt6 protein levels and localization.

A GAG chain polymerization / Tetrasaccharide linkage region / Core protein

Heparan sulfate

Chondroitin sulfate

Dermatan sulfate

B3GAT3 — Glucuronosyl-transferase I
B4GALT7 — Galactosyl-transferase I
B3GALT6 — Galactosyl-transferase II
XYLT1 XYLT2 — Xylosyl-transferase

spEDS-B4GALT7

SEMD-JL1 & spEDS-B3GALT6

Larsen-like syndrome B3GAT3 type

Spondylo-ocular syndrome & Desbuquois dysplasia type 2

Xylose (Xyl) / Glucuronic Acid (GlcA) / N-Acetylgalactosamine (GalNAc)
Galactose (Gal) / N-Acetylglucosamine (GlcNAc) / Iduronic acid (IdoA)
Amino acid / Serine residue

B

H. sapiens B3GALT6 — 2.81 kb — Forward strand

D. rerio b3galt6 — 1.06 kb — Forward strand

C

```
Q96L58 B3GT6_HUMAN    1   MKLLRRAWRRRAALGLGTLALCGAALLYLARCAAEPGDPRAMSGRSP-------PP---P   50
Q256Z7 Q256Z7_DANRE   1   MNLLRLVCRHKTALALGVLLLFAVVLLFLAKCTSETLKPAESPGAAPQAESHQKPPAGPA  60
                          *.****   *.::**.**.* *  ...**:**:*:.*   .*    * :*       **

Q96L58 B3GT6_HUMAN    51  APARAAAFLAVLVASAPRAAERRSVIRSTWLARRGAPGDVWARFAVGTAGLGAEERRALE  110
Q256Z7 Q256Z7_DANRE   61  RPKELSAFLVILITTGPKYTERRSIIRSTWLTKHDPEVLY--WFVIGTEGLPAEDLQNLA  118
                          *  . :***.:*:::.*: :*****.******::.    *.:** ** **:. : *

Q96L58 B3GT6_HUMAN    111 REQARHGDLLLLPALRDAYENLTAKVLAMLAWLDEHVAFEFVLKADDDSFARLDALLAEL  170
Q256Z7 Q256Z7_DANRE   119 TEQIRHHDLLLLPDLRDSYENLTQKLLHMYSWLDQNVEFKFVLKADDDTFARLDLLKEEL  178
                          ** ** ****** ***.***** *.* * .:***::* *:**********.***** *  **

Q96L58 B3GT6_HUMAN    171 RAREPARRRRLYWGFFSGRGRVKPGGRWREAAWQLCDYYLPYALGGGYVLSADLVHYLRL  230
Q256Z7 Q256Z7_DANRE   179 KVKEPK--ERLYWGFFSGRGRVKTAGKWKESAWELCDYYLPYALGGGYVLSADLVRYIRL  236
                          :.:**   .************** .*.:*.:**.**********************.*.*

Q96L58 B3GT6_HUMAN    231 SRDYLRAWHSEDVSLGAWLAPVDVQREHDPRFDTEYRSRGCSNQYLVTHKQSLEDMLEKH  290
Q256Z7 Q256Z7_DANRE   237 NVGFLKIWQSEDVSLGAWLAPVDVKRLHDPRFDTEYKSRGCSNKYLVTHKQSLEDMLEKH  296
                          .  .:*: *:****************.* ********:******:*****************

Q96L58 B3GT6_HUMAN    291 ATLAREGRLCKREVQLRLSYVYDWSAPPSQCCQRREGIP                       329
Q256Z7 Q256Z7_DANRE   297 QTLQRDGRLCKEEVKLRLSYIYDWSVPPSQCCQRKDGIP                       335
                          .**:*****.**:*****.****.*********:.***
```
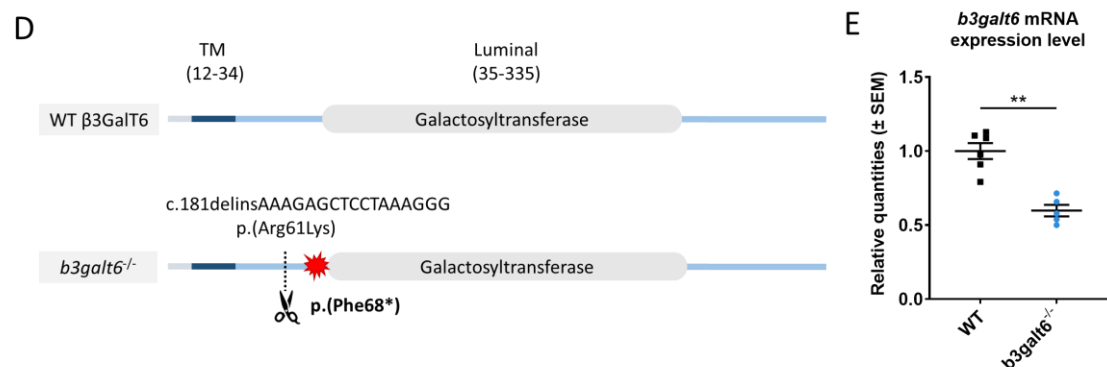
D

TM (12-34)
Luminal (35-335)

WT β3GalT6 — Galactosyltransferase

c.181delinsAAAGAGCTCCTAAAGGG
p.(Arg61Lys)

b3galt6⁻/⁻ — Galactosyltransferase

p.(Phe68*)

E

b3galt6 mRNA expression level

Relative quantities (± SEM)

WT / b3galt6⁻/⁻

**

139

6

140 **Fig. 1. Schematic representation of the GAG biosynthesis and the evolutionary conservation of the zebrafish**

141 **and human *b3galt6/B3GALT6* gene and B3galt6/β3GalT6 protein.** (**A**) Simplified schematic representation of

142 the PG linkage and glycosaminoglycans biosynthesis. PG core proteins are synthesized in the endoplasmic

143 reticulum and undergo further modification in the Golgi apparatus. First, a tetrasaccharide linkage region is

144 synthesized that originates from the addition of a Xyl onto a serine residue of the core protein. Subsequent

145 addition of two Gals and one GlcA residues completes this process. Depending on the addition of GlcNAc or

146 GalNAc to the terminal GlcA residue of the linkage region, HS or CS/DS PGs will be formed, respectively. The

147 elongation of the GAG chain continues by repeated addition of uronic acid and amino sugar residues. The GAG

148 chain is then further modified by epimerization and sulfation (not shown). The main genes encoding for the

149 enzymes involved in the linkage region biosynthesis are indicated in bold and biallelic mutations in these genes

150 result in different linkeropathies. Disorders resulting from deficiency of the enzymes are indicated in black boxes.

151 The deficient enzyme (β3GalT6) and the related disorder studied here are depicted in red (e.g. spEDS-*B3GALT6*

152 and SEMD-JL1). (**B**) Schematic representation of the genomic structure of the *H. sapiens B3GALT6*

153 (NM_080605.4) and *D. rerio b3galt6* (NM_001045225.1) genes. The white and black boxes represent the

154 untranslated regions and the single *B3GALT6/b3galt6* exon, respectively. The zebrafish *b3galt6* gene resides on

155 chromosome 11, spans a region of 1.06 kb and has not been duplicated during teleost evolution. (**C**) Amino acid

156 (AA) sequence alignment (Clustal Omega) between *H. sapiens* β3GalT6 (Uniprot: Q96L58) and *D. rerio* B3galt6

157 (Uniprot: Q256Z7). The luminal galactosyltransferase domain is highlighted in grey. Conservation of AA

158 sequences is shown below the alignment: "*" residues identical in all sequences in the alignment; ":" conserved

159 substitutions; "." semi-conserved substitutions; "space" no conservation. (**D**) Schematic representation of the

160 cmg20 allele in *b3galt6* mutants. *b3galt6* consists of three parts, a cytosolic domain (AA 1-11), a transmembrane

161 domain (TM, AA 12-34) and a luminal domain (AA 35-335). The location of the CRISPR/Cas9-generated indel

162 variant is indicated by a scissor symbol and the resulting premature termination codon (PTC) is depicted by a red

163 star. (**E**) RT-qPCR analysis of relative *b3galt6* mRNA expression levels in *b3galt6*$^{-/-}$ adult zebrafish (0.597 ±

164 0.03919) (n=5) compared to WT siblings (1 ± 0.05395) (n=6). Data are expressed as mean ± SEM. A Mann-Whitney

165 U test was used to determine significance, **P<0.01.

166 To examine the activity of B3galt6 in different *b3galt6*$^{-/-}$ tissues, concentrations of CS, DS and HS

167 disaccharides extracted from bone, muscle and skin from WT and *b3galt6*$^{-/-}$ zebrafish were quantified

168 using a combination of enzymatic digestion and anion-exchange HPLC (Figs. S2-S5 and Tables S1-S4).

169 Overall, a generalized decrease in HS, CS and DS concentration was detected in all examined tissues of

170 *b3galt6*$^{-/-}$ zebrafish. In the GAG fractions prepared from bone, the disaccharide concentration of the

171 CS/DS and CS moieties was significantly decreased by respectively 55% and 64%, compared to WT

172 zebrafish (Table 1 and Tables S1 and S2). DS moieties were undetectable in bone of *b3galt6*$^{-/-}$ zebrafish,

173 whereas their concentration was 50.5 pmol/mg protein in bone of WT zebrafish (Table 1 and Table

174   S3). A non-significant decrease in the disaccharide concentration of the HS moiety was observed in

175   *b3galt6^{-/-}* mutant bone (Table 1 and Table S4), compared to WT. In GAG fractions prepared from

176   *b3galt6^{-/-}* muscle, CS/DS, CS and DS disaccharide moieties were generally lower than in WT muscle

177   (Table 1 and Tables S1-S3). Due to the low concentrations close to the detection limit, a significant

178   reduction could only be detected for the DS moiety (72% reduction) (Table 1 and Table S3). In addition,

179   a significant decrease in HS disaccharide moieties by 56% was noted in *b3galt6^{-/-}* muscle compared to

180   WT muscle (Table 1 and Table S4). In the GAG fractions prepared from *b3galt6^{-/-}* skin, the concentration

181   of all disaccharide moieties was significantly reduced compared to WT (Table 1 and Tables S1-S4). The

182   disaccharide concentration of the CS/DS, CS, DS and HS moieties were decreased by respectively 77%,

183   73%, 55% and 62% compared to WT (Table 1 and Tables S1-S4). No altered sulfation patterns were

184   observed in disaccharide moieties when comparing unique GAG chains between WT and *b3galt6^{-/-}*

185   zebrafish samples (Tables S1-S4).

186   Despite the strong reduction in disaccharide concentrations observed in *b3galt6^{-/-}* zebrafish, low

187   amounts of GAGs were still produced in the mutants. Similar results were obtained for the second

188   *b3galt6* KO zebrafish (cmg22 allele) (Table S5). RT-qPCR revealed no significant upregulation of other

189   galactosyltransferase(s) member(s) from the *b3galt* family (*b3galt1a*, *b3galt2*, *b3galt4*, *b3galnt2*) or of

190   other linkage-enzymes (*xylt1*, *xylt2*, *b4galt7* and *b3gat3*) (Fig. S6), suggesting that altered expression

191   of these genes did not compensate for the reduced *b3galt6* mRNA levels.

192   **Table 1. Concentrations of GAG disaccharides in wild-type and *b3galt6^{-/-}* zebrafish tissues**

	pmol/mg protein (Average $\pm$ SE)			
	CS/DS	CS	DS	HS
Bone				
Wild-type	774.2 ± 19.9	728.4 ± 148.1	50.5 ± 8.1	178.6 ± 19.8
b3galt6^{-/-}	$346.1 \pm 20.0^{*}$	$279.9 \pm 4.8^{**}$	N.D.	137.1 ± 39.7^{ns}
Muscle				
Wild-type	9.3 ± 0.4	2.1 ± 0.4	14.5 ± 1.1	30.8 ± 1.2
b3galt6^{-/-}	5.7 ± 3.1^{ns}	N.D.	$4.1 \pm 1.0^{*}$	$13.5 \pm 4.0^{**}$
Skin				
Wild-type	236.2 ± 26.5	175.1 ± 25.3	75.9 ± 7.9	55.1 ± 4.5
b3galt6^{-/-}	$55.4 \pm 15.2^{*}$	$47.9 \pm 13.5^{**}$	$33.8 \pm 6.3^{**}$	$21.0 \pm 2.8^{**}$

193   Student's t-test (vs wild-type) (n=3), N.D.: not detected (<1 pmol/mg protein), *P<0.01, **P<0.05, ns: not

194   significant, SE: standard error.

B3galt6-deficiency leads to the biosynthesis of a non-canonical (GlcA-Gal-Xyl-*O*-) trisaccharide linkage region in zebrafish

In order to explain why *b3galt6*^{-/-} zebrafish can still produce GAG chains on PG core proteins, we investigated the composition of the linkage region. To this purpose, whole zebrafish extracts were enriched for all proteoglycans, their GAG chains depolymerized with bacterial lyases, the core proteins digested with trypsin and the remaining glycopeptides subjected to nano-scale liquid chromatography-tandem mass spectrometry (nLC-MS/MS) using a recently developed glycoproteomic approach [27, 28]. Potential structural differences in PG linkage regions in WT versus *b3galt6*^{-/-} zebrafish are thus elucidated through the combined identities of peptide backbones and GAG linkage region structures. The glycoproteomic analysis identified two CS-glycopeptides derived from biglycan (UniProt: A8BBH0) in both the WT and *b3galt6*^{-/-} zebrafish. These CS-glycopeptides displayed different linkage region structures in WT compared with *b3galt6*^{-/-} zebrafish (Fig. 2). While the peptide in the WT zebrafish was modified with a hexasaccharide structure (Fig. 2A), the peptide in the *b3galt6*^{-/-} zebrafish was modified with a pentasaccharide structure (Fig. 2B), supporting the hypothesis that *b3galt6*^{-/-} zebrafish produces a non-canonical trisaccharide linkage region. The precursor ion (m/z 1281.7922; 3+) in the WT zebrafish equated to a mass of a peptide (DQEEGSAVEPYKPEHPTCPFGCR) modified with a hexasaccharide structure, with the peptide containing two carbamidomethyl (CAM) modifications. Furthermore, the hexasaccharide structure was modified with one sulfate group (SO_3^-) on the subterminal GalNAc residue [GlcAGalNAc-H_2O+SO_3+H]$^+$, and one phosphate group (HPO_3^-) on the Xyl residue (Fig. S7). In contrast, the precursor ion (*m/z* 1227.7765; 3+) in the *b3galt6*^{-/-} zebrafish equated to a mass of the same peptide but modified with a pentasaccharide structure, with two phosphate/sulfate groups, with the peptide containing two CAM modifications. The difference in mass between the WT and *b3galt6*^{-/-} precursor ions corresponds to 162.08 Da, equating to the mass of a hexose (galactose) residue (162 Da). Additional HS- and CS- glycopeptides with the expected tetrasaccharide linkage region were found in the WT. In the *b3galt6*^{-/-}, no HS-modified structures were identified but additional CS-glycopeptides with the non-canonical trisaccharide linkage region were found. Table S6 shows a complete list of all glycopeptides identified in both WT and *b3galt6*^{-/-} zebrafish. PGs harboring a tetrasaccharide linkage region were never detected in the *b3galt6*^{-/-} adult zebrafish samples and no trisaccharide linkage region was detected in WT zebrafish samples.

These observations suggest that B3GAT3/GlcAT-I can transfer a GlcA residue not only to Gal-Gal-Xyl, but also to a Gal-Xyl substrate. This was confirmed by an *in vitro* GlcAT-I assay, which showed that GlcAT-I is indeed capable of adding a GlcA to a Gal-Xyl-*p*-nitrophynyl, which was chemically synthesized, thus to a substrate ending with a single galactose (Fig. S8).
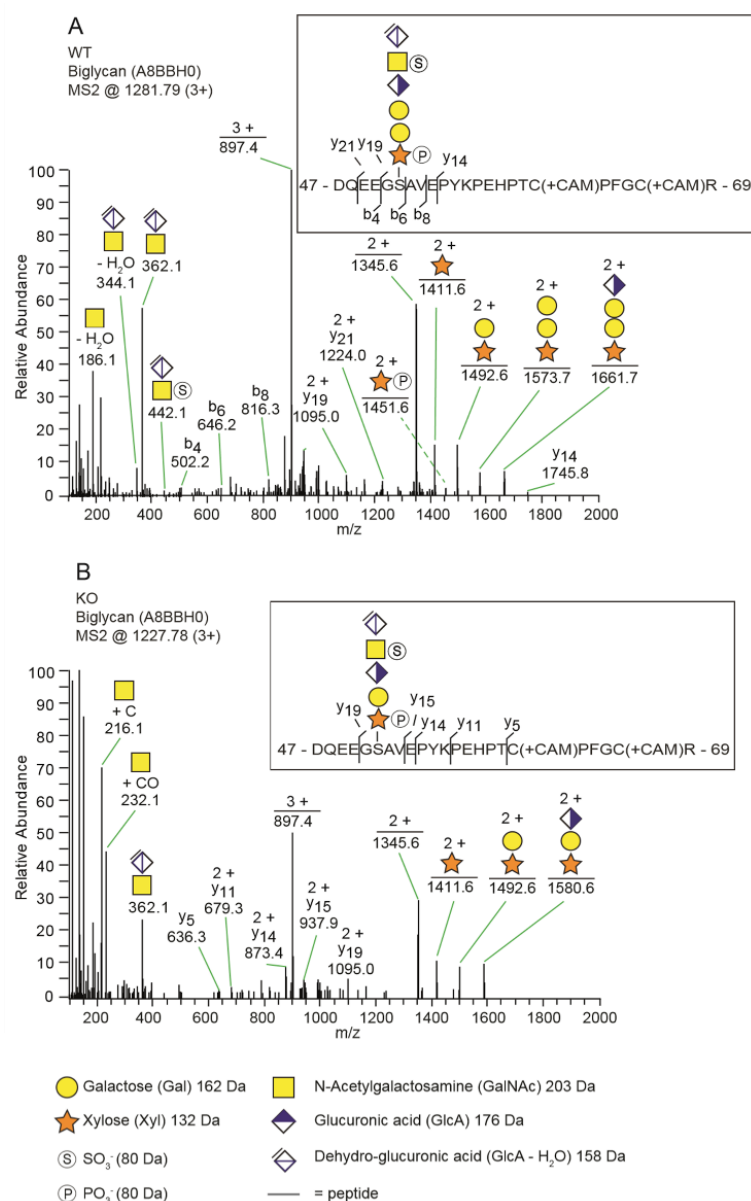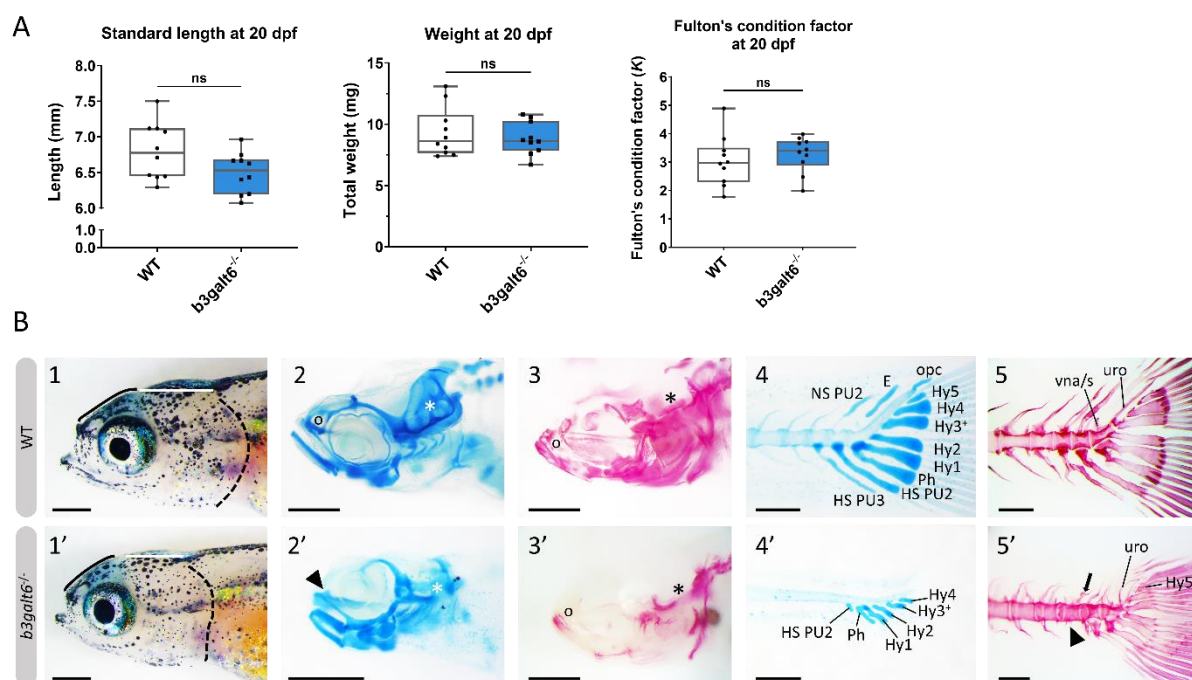
9

Fig. 2. The identification of a trisaccharide linkage region in the *b3galt6*^{-/-} zebrafish. (**A** and **B**) MS2 fragment mass spectra of CS-glycopeptides derived from biglycan (UniProt: A8BBH0) showed different linkage regions in WT compared to the *b3galt6*^{-/-} zebrafish. (**A**) The peptide (DQEEGSAVEPYKPEHPTCPFGCR) in WT zebrafish was modified with a residual hexasaccharide structure, corresponding to the canonical tetrasaccharide linkage region (m/z 1281.79; 3+). The hexasaccharide structure was modified with one sulfate group (SO_3^-) at the subterminal GalNAc residue and one phosphate group (HPO_3^-) at the xylose residue (Fig. S7) (**B**) The peptide (DQEEGSAVEPYKPEHPTCPFGCR) in *b3galt6*^{-/-} zebrafish was modified with a residual pentasaccharide structure, corresponding to a non-canonical trisaccharide linkage region (m/z 1227.78; 3+). The pentasaccharide structure was modified with two phosphate/sulfate groups. Their exact positioning and identity could not be determined due to low intensities of corresponding ion peaks, and the positions are therefore assigned in analogy of the WT structure.

10

240

241 ***b3galt6*^{-/-} zebrafish show early-onset, progressive morphological abnormalities and delay of**

242 **cartilage and bone formation, reminiscent of human spEDS-*B3GALT6***

243 One of the clinical hallmarks of human spEDS-*B3GALT6* is the pronounced skeletal involvement with

244 the presence of spondyloepimetaphyseal dysplasia with postnatal growth restriction, bowing of long

245 bones, hypoplasia of iliac bones, femoral head dysplasia, vertebral body changes, kyphoscoliosis and

246 bone fragility with spontaneous fractures (Table 2). To evaluate the development of cartilage and bone

247 associated with B3galt6-deficiency in zebrafish, phenotypic characterization of *b3galt6*^{-/-} zebrafish was

248 performed in juvenile (20 dpf, days post fertilization) and adult stages (four months).

249 At 20 dpf, the average weight (W), standard length (SL) and Fulton's condition factor (K), which is used

250 as a measure for the relative proportion of SL to W [29], were not significantly different between

251 *b3galt6*^{-/-} and WT siblings (Fig. 3A), although for SL there was a trend towards smaller mutants

252 (P=0.0640). Several externally visible morphological anomalies could be observed in 20 dpf *b3galt6*^{-/-}

253 zebrafish as compared to their WT siblings, including a shorter, more compact head, a shorter and

254 rounder frontal region, a shorter parietal/occipital region and a malformed posterior edge of the

255 opercular apparatus (Fig. 3B). Alcian blue (AB) cartilage staining showed no morphological

256 abnormalities, but developmental delay of the head and pectoral and caudal fin endoskeleton was

257 noted (Fig. 3B, Table S7), with cartilage elements being absent or in early development in *b3galt6* KO,

258 while these structures were already fully developed in WT sibling zebrafish. Alizarin red (AR) mineral

259 staining showed delayed mineralization in all regions of the head, the pectoral fin girdle and the caudal

260 fin (Fig. 3B, Table S8), further confirming developmental retardation. In addition, malformations of

261 different mineralized bones, such as the parasphenoid, branchiostegal rays, supracleithrum and the

262 subopercle bone could be detected in the head of *b3galt6*^{-/-} zebrafish larvae (Fig. S9). The vertebral

263 column, i.e. the vertebral centra and their associated elements (neural and haemal arches), did not

264 show delayed mineralization in *b3galt6*^{-/-} zebrafish larvae, but malformation of the associated

265 elements and fusions of preural vertebrae were observed at a much higher frequency in the *b3galt6*^{-/-}

266 mutants. Kyphosis, scoliosis and lordosis were also more frequently observed and pronounced in

267 *b3galt6*^{-/-} larvae compared to WT siblings (Fig. S10 & Table S8). A similar phenotype was observed in

268 the second *b3galt6* KO model (cmg22 allele), confirming the specificity of the displayed phenotype

269 (Fig. S11).

11

Fig. 3. Developmental delay and morphological abnormalities in 20 dpf *b3galt6*^{-/-} zebrafish. (**A**) Weight, standard length and Fulton's condition factor of WT and *b3galt6*^{-/-} zebrafish larvae at 20 dpf (n=10). (**B**) External phenotype of the head of juvenile WT and *b3galt6*^{-/-} sibling zebrafish. All images are oriented anterior to the left, posterior to the right, dorsal to the top and ventral to the bottom. (**1-1'**) *b3galt6*^{-/-} zebrafish display a rounder frontal region (black line), shorter parietal/occipital region (white horizontal line) and a malformed posterior edge of the opercular apparatus (dotted black line), compared to WT control. (**2-2'**) Representative images of cartilage AB staining of the head. The olfactory region (indicated by 'o' in the WT and arrowhead in the *b3galt6*^{-/-} picture) and the otic region (indicated by white asterisk) show delayed development of cartilage elements in *b3galt6*^{-/-} zebrafish as compared to WT. (**3-3'**) Representative images of AR mineral staining of the head. The olfactory region (indicated by 'o') and the otic region (indicated by asterisk) show severely delayed mineralization in *b3galt6*^{-/-} zebrafish larvae as compared to WT. (**4-4'**) Representative images of AB staining of the caudal fin. The modified associated elements show developmental delay in *b3galt6*^{-/-} zebrafish as compared to WT. Abbreviations: E, epural; HS PU2, haemal spine of preural 2; HS PU3, haemal spine of preural 3; Hy1-5, hypural 1-5; NS PU2, neural spine preural 2; opc, opistural cartilage; Ph, parhypural (**5-5'**) Representative images of AR mineral staining of the caudal fin. Caudal vertebrae and their associated elements show no delay in ossification. Malformation or absence of caudal fin associated elements (block arrow indicates a neural arch; arrowhead indicates a missing haemal arch), and malformation of uroneural (uro) and vestigial neural arches and spines (vna/s) are observed in *b3galt6*^{-/-} zebrafish; hypurals have a bent appearance. Scale bars: images of the head 500 µm, images of the caudal fin 200 µm.

12

291   At the adult stage (four months), *b3galt6*$^{-/-}$ zebrafish had a significantly reduced average SL (1.834 ±

292   0.077 cm), and W (0.1196 ± 0.014 g), when compared to their WT siblings (2.371 ± 0.049 cm, and

293   0.2497 ± 0.016 g, respectively), while the Fulton's condition factor (*K*) indicated that SL and W were

294   normally proportioned to each other (Fig. 4A). A similar phenotype was observed in the second *b3galt6*

295   KO model (cmg22 allele), confirming the specificity of the displayed phenotype (Fig. S1).

296   The head malformations, which were already observed in 20 dpf *b3galt6*$^{-/-}$zebrafish, showed further

297   progression, with a more pronounced smaller, rounded head and an abnormal compaction of the

298   opercular apparatus (Fig. 4B). In addition, a reduced surface area of the fins, with a crenelated postero-

299   distal fin edge was observed in the mutant animals. The pectoral fins were pointing in an abnormal

300   upwards angle (Fig. 4B). Kyphoscoliosis was variably present and mainly occurred in the posterior part

301   of the body (not shown). In addition, an altered pigmentation pattern was observed, mainly on the

302   ventral part of the body where the dark stripes showed interruptions (Fig. 4B).

303

13
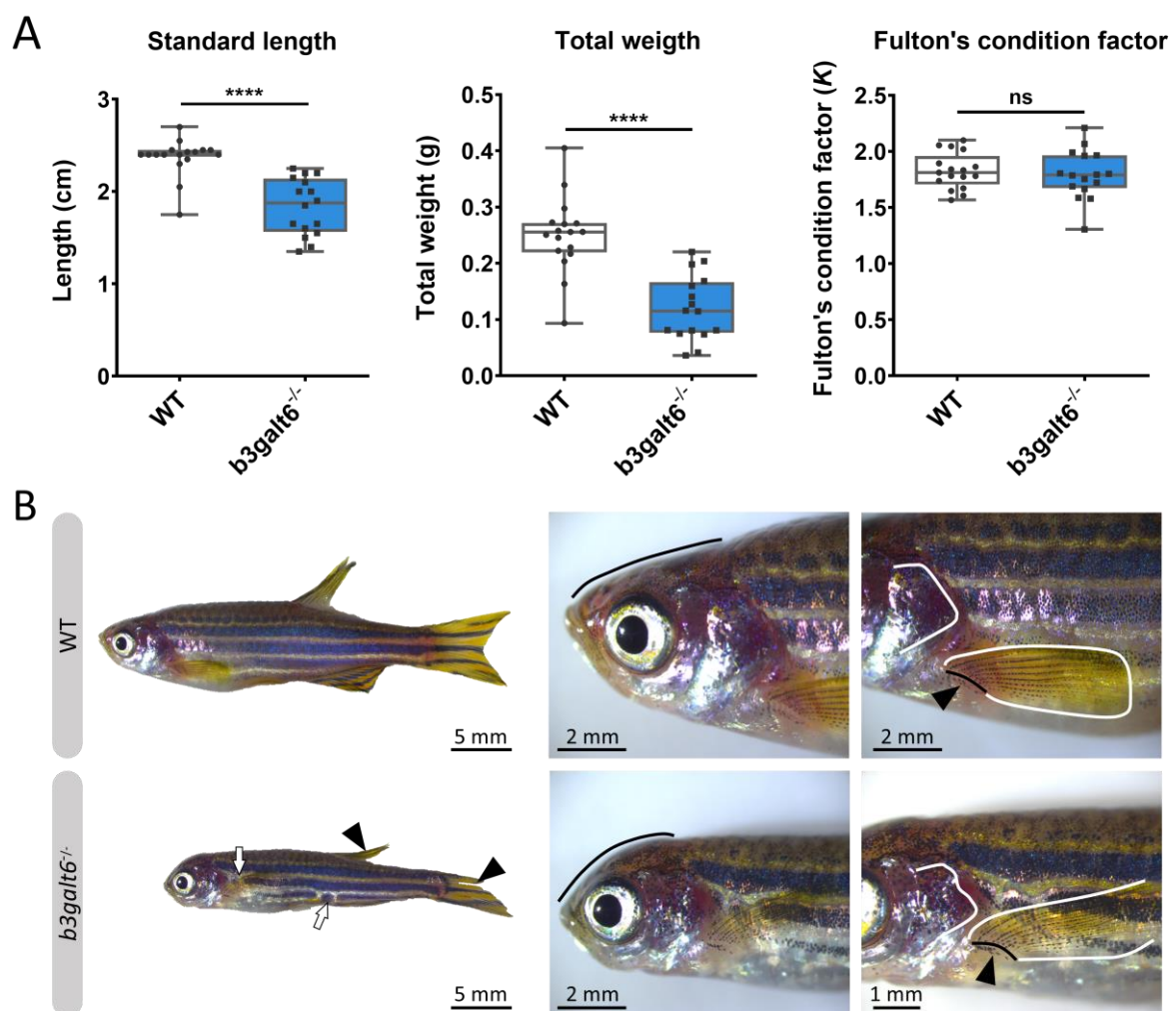
304 **Fig. 4. Characterization of the external phenotype of adult _b3galt6-/-_ zebrafish.** (**A**) _b3galt6-/-_ zebrafish (n=16)

305 had a significantly shorter standard length (SL) compared to their WT siblings (n=17). The weight (W) was

306 significantly lower in the mutant zebrafish. The Fulton's condition factor (K= 100*(W/SL^3)) was not significantly

307 different between _b3galt6-/-_ zebrafish and WT siblings. Data are expressed as box plots with min-to-max whiskers

308 on which each individual data point is plotted. An unpaired t-test with Welch's correction was used to determine

309 significance. ****P<0.0001, ns: not significant. (**B**) Adult _b3galt6-/-_ zebrafish exhibit morphological abnormalities

310 compared to their WT siblings; _b3galt6-/-_ zebrafish display interruptions of the blue horizontal stripes (white

311 arrows), smaller fins (arrowhead), aberrations of the head shape (black line), of the shape of the opercular

312 apparatus (white line indicates the posterior edge) and of the pectoral fin (black line and arrow indicate the fin

313 rays at the base of the fin, white line shows the outline of the fin).

314 Further progression of the larval phenotype was also confirmed by AR staining of the mineralized

315 skeleton in adult (four months) _b3galt6-/-_ zebrafish. The olfactory region was underdeveloped (Fig. 5A),

316 the cranial roof bones and sutures were deformed (Fig. S12) and the opercular apparatus was smaller

317 and compacted in KO zebrafish (Fig. 5A and Fig. S12). The fifth ceratobranchial arch and its attached

318 teeth were smaller in _b3galt6-/-_ zebrafish (Fig. 5B). In the pectoral fins of _b3galt6-/-_ zebrafish the radials

319 were smaller, had an irregular shape, and were often fused (Fig. 5B). The autocentra, i.e. the inner

320 layer of the vertebral centra in the vertebral column and caudal fin [30] of KO zebrafish had a normal

321 hourglass shape, but the associated elements often showed presence of extra intramembranous bone

322 (Fig. 5 and Fig. S12) and extra bony elements (Fig. 5A). Fusions were observed in preural vertebrae (Fig.

323 5A). Lordosis, kyphosis and scoliosis was variably observed along the vertebral column of _b3galt6-/-_

324 mutant zebrafish (not shown). Extra mineralization was observed at the edge (growth zone) of _b3galt6-/-_

325 scales (Fig. 5B). Notably, variation in the severity of the skeletal malformations in _b3galt6-/-_ zebrafish
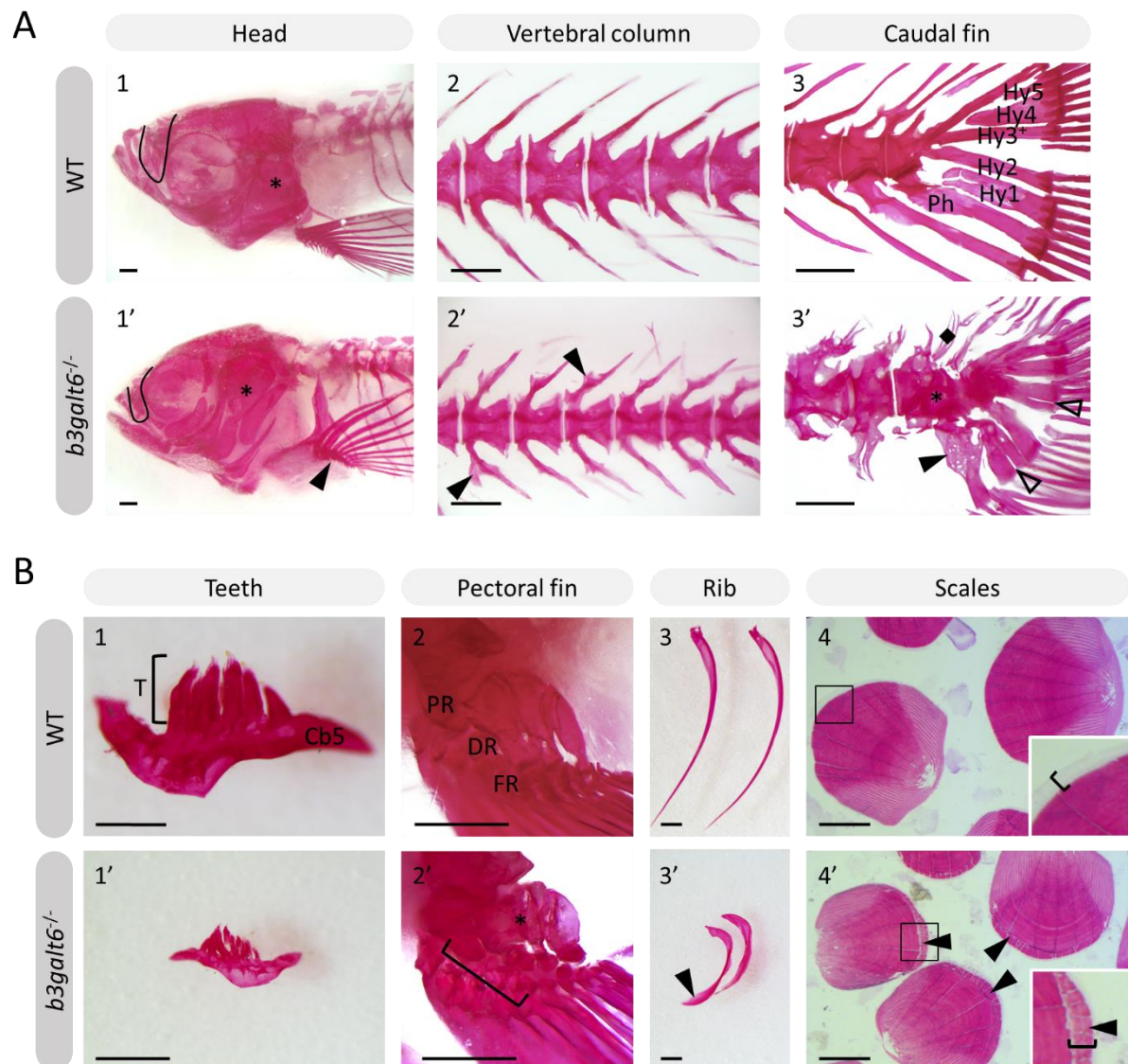
326 was observed.

14

Fig. 5. Alizarin red stained mineralized bone in WT and *b3galt6*$^{-/-}$ adult zebrafish. The mineralized bones in the skeleton were studied in four-month-old WT and mutant zebrafish after AR mineral staining. (**A**) *b3galt6*$^{-/-}$ zebrafish display malformation of the cranium, vertebral column and caudal fin. (**A1-1'**) The cranium shows an underdeveloped olfactory region (black line) and a smaller compacted opercular bone (asterisk). (**A2-2'**) The vertebral column shows extra intramembranous outgrowths located where the distal tip of the neural and haemal arches fuse to neural and haemal spine respectively (arrowheads). (**A3-3'**) In the caudal fin fusion of preural vertebrae is observed (asterisk). Associated elements show intramembranous outgrowths (arrowhead) and the presence of extra bony elements (diamond). The distal tip of the hypurals is sometimes split (transparent arrowhead). Structures indicated in the WT caudal fin: Hy1-5, hypural 1-5, Ph, parhypural. (**B**) Details of mineralized structures in *b3galt6*$^{-/-}$ zebrafish. (**B1-1'**) The fifth ceratobranchial arch and its teeth are smaller in KO zebrafish. (**B2-2'**) The proximal (PR) and distal radials (DR) have irregular shapes in mutant zebrafish. Proximal (asterisk) and distal radials are sometimes fused. The bracket indicates a fusion between a proximal and distal

15

340   radial, and the first fin ray (FR). (**B3-3'**) Ribs also show extra intramembranous bone (black arrowhead). (**B4-4'**)

341   More mineralization was observed at the growth zone (bracket) of the scales in mutant zebrafish (arrowhead).

342   Scale bars = 500 μm.

343   Subsequent quantitative μCT analysis of four-month-old zebrafish revealed multifaceted effects of

344   B3galt6-deficiency on vertebral morphology and mineralization. Most notably, the volume of vertebral

345   centrum, haemal and neural associated elements was significantly reduced throughout the entire

346   vertebral column in *b3galt6*$^{-/-}$ zebrafish (P<0.01), with more pronounced differences in the abdominal

347   region (Fig. 6). Tissue mineral density (TMD) was not significantly different in the *b3galt6*$^{-/-}$ vertebral

348   bodies compared to WT siblings. However, TMD in zebrafish is proportionally related to standard

349   length [31, 32], and *b3galt6*$^{-/-}$ zebrafish exhibited a significantly reduced body size compared to the

350   WT siblings. We therefore normalized the μCT data to standard length using the normalization

351   procedure outlined by Hur *et al.* [33]. In this procedure, phenotypic data in WT sibling controls was

352   scaled using the mean standard length of *b3galt6*$^{-/-}$ zebrafish as the reference length. Remarkably,

353   after normalization, a significant increase in TMD of centrum, haemal and neural associated elements

354   was noted in *b3galt6*$^{-/-}$ zebrafish compared to WT controls (P<0.001, P<0.01 and P<0.01, respectively)
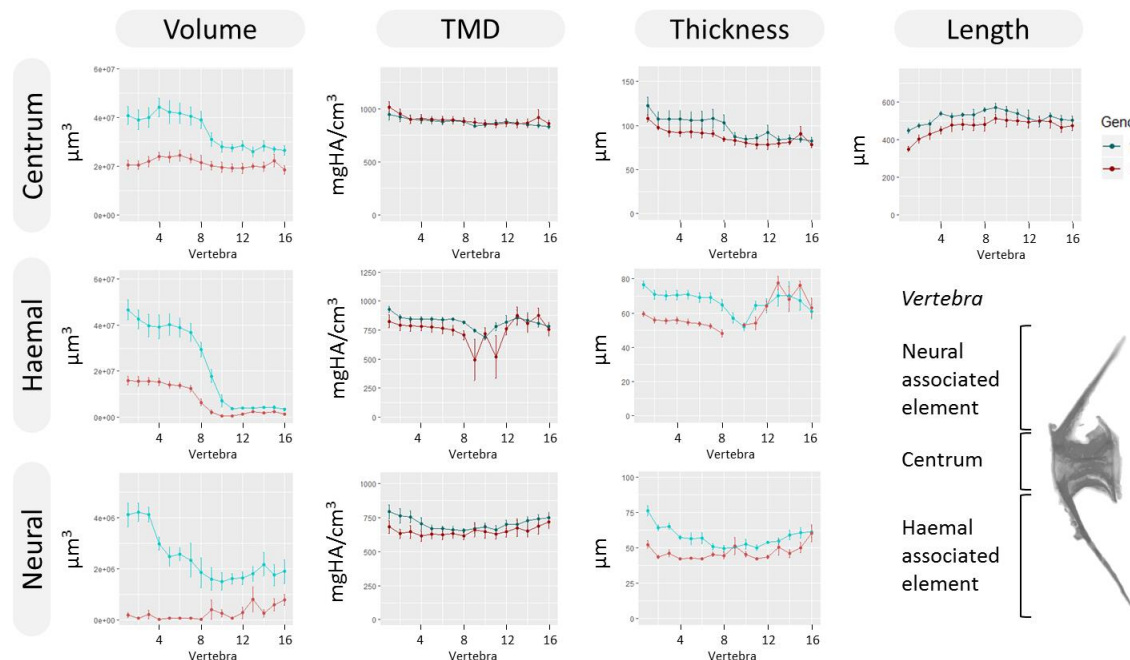
355   (Fig. S13).

356

357   **Fig. 6. μCT analysis of adult WT and *b3galt6*$^{-/-}$ zebrafish.** Quantitative μCT analysis of the vertebral column in

358   five mutant versus five WT zebrafish at the age of four months. The bone volume, tissue mineral density (TMD)

359   and bone thickness were calculated for three parts of each vertebra: the vertebral centrum, the neural associated

16

360　element (neural arch and neural spine) and the haemal associated element (haemal arch and haemal spine).

361　Plots associated with a significant difference are colored in a lighter coloring scheme. The X-axis represents each

362　vertebra along the anterior-posterior axis. The volume is significantly reduced for each part of the vertebra in

363　$b3galt6^{-/-}$ zebrafish (P<0.01, P<0.001 and P<0.000001, respectively). The thickness of the haemal (P<0.01) and

364　neural (P=0.001) associated element is also significantly reduced in the mutants whereas the centrum thickness

365　is not significantly reduced in $b3galt6^{-/-}$ zebrafish (P=0.12). TMD is not significantly different between $b3galt6^{-/-}$

366　zebrafish and WT siblings when not normalized for standard length (P>0.2). Data are presented as mean ± SEM.

367　TMD, tissue mineral density; HA, hydroxyapatite.

$b3galt6$ knock-out zebrafish display a disturbed organization of type I collagen fibrils in skin, bone and intervertebral space

370　Transmission electron microscopy (TEM) studies on the dermis of spEDS-$B3GALT6$ patients revealed

371　an abnormal collagen fibril architecture with loosely packed collagen fibrils of variable size and shape

372　[5]. We therefore studied the effect of loss of galactosyltransferase II activity on collagen fibril

373　architecture. TEM sections of skin biopsies of $b3galt6^{-/-}$ zebrafish showed an abnormal dermal collagen

374　fibril architecture characterized by loosely packed collagen fibrils and larger and more interfibrillar

375　spaces compared to WT siblings (Fig. 7A). In addition, at the level of the scales a thicker epidermal

376　layer was observed and electron dense structures were present in the interfibrillar spaces (Fig. 7A).

377　Next, we examined the intervertebral region and adjacent vertebral centra in the vertebral column of

378　five-month-old zebrafish by means of TEM. In general, the type I collagen fibers in $b3galt6^{-/-}$ zebrafish

379　displayed a lower degree of organization (Fig. 7B). This was observed in immature collagen layers,

380　deposited by osteoblasts in the outer edges of the intervertebral space, but also in the mature type I

381　collagen layers of the intervertebral ligament and in the autocentrum, the inner layer of the vertebral

382　bone, where a lack of the typical plywood-like organization was seen. Detailed investigation of TEM

383　sections of the vertebral bone revealed presence of several electron dense spots of unknown origin in

384　knock-outs. These 'dark spots' may reflect extrafibrillar hydroxyapatite crystals (Fig. 7B).

385　Mass spectrometry analysis of type I collagen modification in bone derived from the vertebral column

386　showed no significant difference in hydroxylation status of the α1(I) K87 and C-telopeptide lysine

387　residues (Table S9). These lysine residues are conserved in zebrafish and human type I collagen and

388　are crucial for intermolecular crosslinking of collagen fibrils in bone matrix [34].
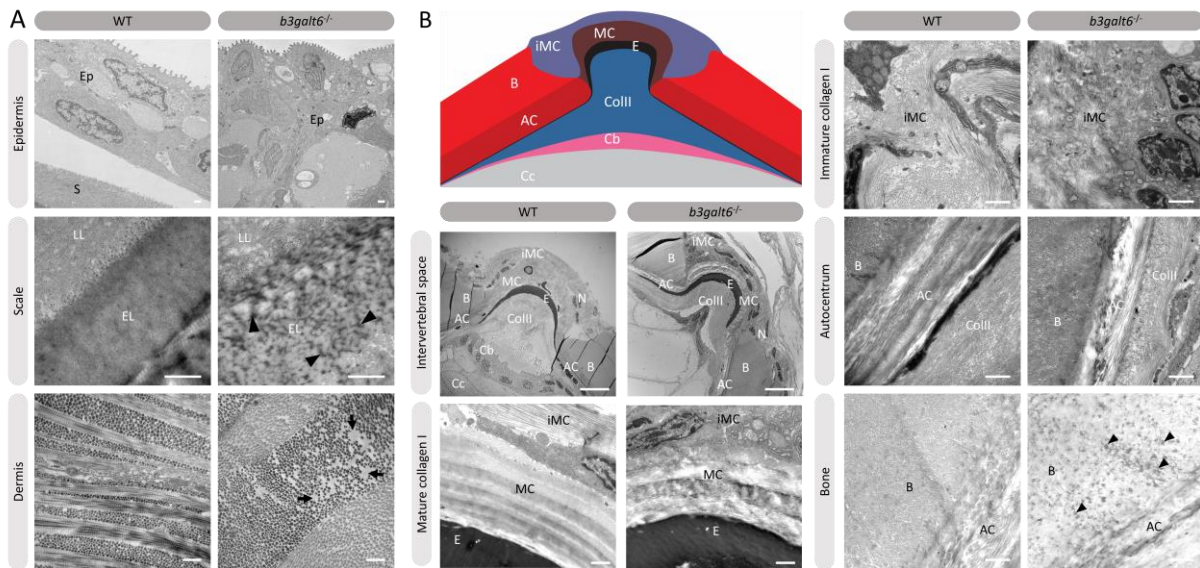
17

Fig. 7. Collagen fibrillar architecture in five-month-old adult zebrafish. (**A**) Skin from five-month-old WT and *b3galt6*^{-/-} adult zebrafish. The epidermis (Ep), the outer layer of the skin covering the scales (S) of zebrafish, appears thicker in *b3galt6*^{-/-} zebrafish compared to the epidermis of WT zebrafish. A mature zebrafish scale consists of several layers. The limiting layer of the scale (LL) is rich in fine granules that in some areas are linearly arranged, forming dense layers. This matrix contrasts with that of the external layer(s) (EL) below. Structures resembling extrafibrillar crystals (arrowhead) are noted in the external layer of the mutant scale, which are rare in WT zebrafish sections. Upon investigation of the dermis of *b3galt6*^{-/-} mutants, increased interfibrillar spaces are noted (arrows), which are absent in the dermis of WT adults. Scale bars = 500 nm. (**B**) Schematic representation and TEM images of the zebrafish intervertebral space. Schematic representation of the zebrafish intervertebral space. Abbreviations: AC, autocentrum; B, bone; Cb, chordoblasts; Cc, chordocytes; ColII, type II collagen; E, elastin; iMC, immature collagen type I layer; MC, mature collagen type I layer. Starting from the central body axis, several recognizable structures are present in the intervertebral space along a proximo-distal axis: (i) notochord tissue consisting of chordocytes and chordoblasts, (ii) the notochord sheath consisting of a type II collagen layer and an external elastic membrane, (iii) and a connective tissue ligament consistent of a mature and an immature type I collagen layer. The mature type I collagen layer is organized in a typical plywood-like pattern and is continuous with the inner layer of the vertebral bone, i.e. the autocentrum, which also shows a plywood-like organization. The immature type I collagen layers consist of loose collagen fibers connecting the outer layer of vertebral bones. Notice the higher number of nuclei (N) in the *b3galt6*^{-/-} zebrafish at the intervertebral space. Mature collagen (MC) displays a typical plywood-like organization, in WT zebrafish but not in comparable regions for *b3galt6*^{-/-} mutant zebrafish. Cross section and longitudinal type I collagen regions are less clearly demarcated and smaller in immature collagen (iMC) from *b3galt6*^{-/-} zebrafish compared to WT siblings. It is more difficult to pinpoint the different layers of the autocentrum (AC) in the KO compared to WT

18

412 zebrafish. Bone (B) from the *b3galt6*$^{-/-}$ zebrafish shows electron dense structures (arrowhead). Scale bars = 10

413 μm for the intervertebral space and 1 μm for the other images.

b3galt6 knock-out zebrafish display ultrastructural muscle abnormalities and lower endurance

415 Human spEDS-*B3GALT6* patients often suffer from muscle hypotonia with a delay in motor

416 development. In view of the observed reduction in the concentration of the different GAG moieties in

417 muscle of *b3galt6*$^{-/-}$ zebrafish, we investigated the function and the ultrastructural appearance of

418 muscle.

419 First, the critical swimming speed (U_{crit}) and endurance of the zebrafish were assessed by means of a

420 custom-made swim tunnel. The U_{crit}, defined as the maximum velocity that the tested zebrafish could

421 sustain for at least 5 minutes [35], was significantly lower in *b3galt6*$^{-/-}$ zebrafish (30.1 ± 2.39 cm/s)

422 compared to length-matched WT (41.61 ± 1.942cm/s) (P<0.01) (Fig. 8A). The stamina of each zebrafish

423 was determined by an effort test where it was tested how long zebrafish could swim at high speed (37

424 cm/s) after a three-minute warm-up. This effort test showed that the *b3galt6*$^{-/-}$ zebrafish performed

425 less well compared to length-matched WT zebrafish, indicating a lower endurance (Fig. 8B).

426 The muscle tissue in the zebrafish trunk was further investigated at the ultrastructural level. Toluidine

427 blue-stained semi-thin cross sections revealed that the endomysium, a layer of connective tissue

428 ensheating the muscle fibers, was enlarged along the horizontal myoseptum of *b3galt6*$^{-/-}$ zebrafish,

429 although no clear differences in muscle fiber diameter were noted (Fig. 8C). Ultra-thin parasaggital

430 sections, investigated by TEM, showed that the length of the sarcomeres, the smallest basic units of

431 striated muscle, as well as the length of the A and I band were significantly increased in the *b3galt6*$^{-/-}$

432 zebrafish (Fig. 8D).
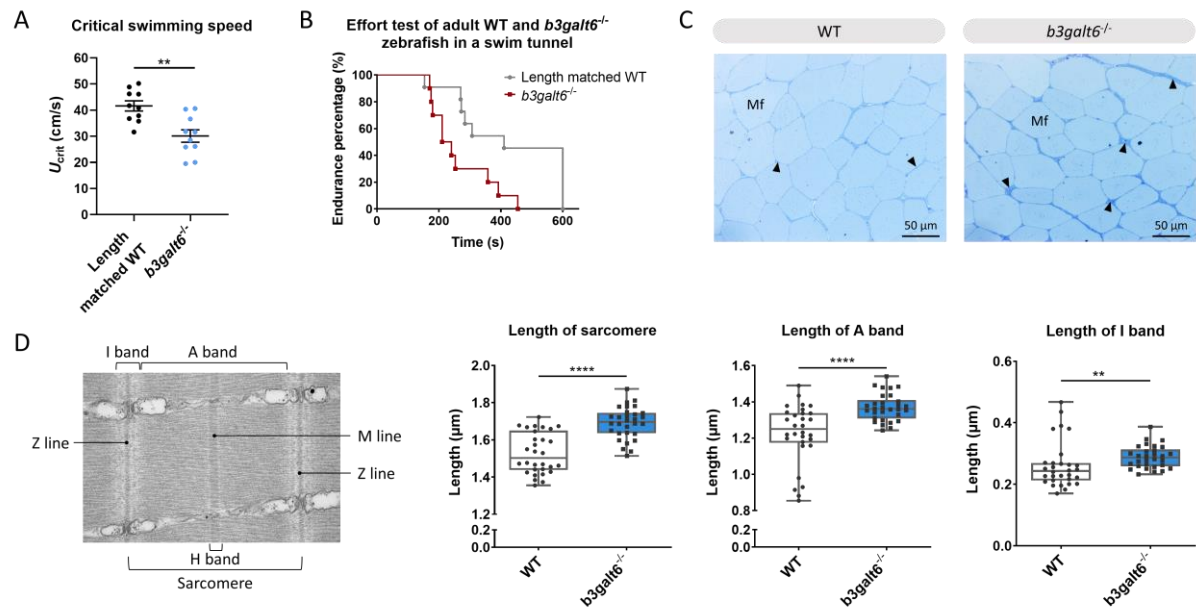
Fig. 8. Functional and structural analysis of adult WT and *b3galt6*-/- zebrafish muscle. (**A**) The critical swimming speed and (**B**) the endurance performance was determined for *b3galt6*-/- and length-matched WT zebrafish. (**C**) Semi-thin cross sections, stained with toluidine blue, demonstrate the presence of a thicker endomysium (arrowhead), located between the muscle fibers (Mf) at the horizontal myoseptum of *b3galt6*-/- zebrafish at the age of five months. (**D**) Transmission electron microscope structure of a sarcomere with indications of the Z and M line and A, I and H band. The sarcomere length was determined at 5 different loci per semi-thin section, for 6 semi-thin originating coming from 3 different zebrafish per genotype (N=30). A significant increase in sarcomere length for *b3galt6*-/- is noted. Furthermore, both the A and I band show an increase in length for the mutant zebrafish. Data are expressed as box plots with min-to-max whiskers on which each individual data point is plotted. A Mann-Whitney U test was used to determine significance. ****$P<0.0001$, **$P<0.01$.

Discussion

In this study we developed two viable *b3galt6* KO zebrafish models using CRISPR/Cas9 mutagenesis, and performed an in-depth characterization of the biochemical, ultrastructural and phenotypical consequences of β3GalT6-deficiency on different tissues, including skin, cartilage, mineralized bone and muscle. These models currently represent the only vertebrate models available for the study of the pathogenetic consequences of β3GalT6-deficiency on tissue development and homeostasis. In both models we detected a significant reduction, yet not a complete absence in *b3galt6* mRNA expression (Fig. 1E). One possible explanation is the absence of canonical nonsense-mediated decay (NMD) in the single-exon *b3galt6* gene, due to a lack of exon junction complexes (EJCs) [36]. We were unable to examine the effect of the mutations on B3galt6 protein levels and localization due to the

20

455   unavailability of a suitable antibody. Nevertheless, since the cmg20 and cmg22 alleles are predicted to

456   introduce a PTC respectively upstream and in the catalytic domain, residual translation of some mRNA

457   into a truncated protein is not expected to lead to the production of an active enzyme. β3galt6 is a key

458   enzyme in the biosynthesis of the common linkage region of PGs, and reduced levels of active enzyme

459   are thus expected to equally affect the biosynthesis of HS and CS/DS GAG chains. We therefore

460   quantified the disaccharide concentrations in bone, muscle and skin of adult *b3galt6*$^{-/-}$ zebrafish by

461   means of a combination of enzymatic digestion and anion-exchange HPLC. This revealed a distinct, and

462   relatively proportional decrease in the concentration of CS, DS, hybrid CS/DS and HS moieties in all

463   examined tissues, compared to age-matched WT zebrafish (Table 1). Nonetheless, low amounts of

464   GAGs were still produced in the KO zebrafish in absence of upregulation of other galactosyltransferase

465   member(s) from the *b3galt* family or by other linkage-enzymes (Fig. S6). Together with the previous

466   demonstration that the other five β3GalT human enzymes (e.g. β3GalT1, β3GalT2,

467   β3GalT3/β3GalNAcT1, β3GalT4 and β3GalT5) are involved in the biosynthesis of glycoproteins and

468   glycolipids [11], compensation for galactosyltransferase II deficiency in zebrafish by other *b3galt* family

469   members is unlikely. Chinese hamster ovary *B3galt6* KO cells were also shown to be capable of

470   producing GAGs, in contrast to *Xylt2*, *B4galt7* or *B3gat3* KO cells [37]. The recent identification of the

471   presence of a non-canonical trisaccharide linkage region, lacking one Gal residue (GlcA-Gal-Xyl-*O*-), as

472   a minor constituent in the PG bikunin in the urine of healthy human individuals [28], prompted us to

473   examine the composition of the GAG linkage region in our *b3galt6* KO zebrafish models, by analyzing

474   protein extracts from adult *b3galt6*$^{-/-}$ and WT zebrafish via LC-MS/MS. This led to the striking finding

475   that the few detected PGs in the *b3galt6*$^{-/-}$ zebrafish all presented with a trisaccharide PG linkage

476   region, consisting of only one Gal (Fig. 2B) (Table S6). Further *in vitro* analysis indicated that GlcAT-

477   I/B3GAT3 is capable of adding a GlcA to Gal-Xyl-*O*- (Fig. S8). This observation might explain the

478   phenotypic differences observed between GalT-II/B3GALT6 deficiency and deficiencies of the other

479   linkage region enzymes, for which such a rescue mechanism might be absent. This hypothesis is

480   supported by the lack of GAGs in the Chinese hamster ovary *Xylt2*, *B4galt7* or *B3gat3* KO cells and by

481   the lethal phenotype observed in the *b4galt7* KO zebrafish model [38]. At present, we have no

482   information on the length of the GAG chains attached to the trisaccharide linkage region or the

483   composition and the possible modifications of these HS and CS/DS chains. As such, the GAG structure,

484   length and modifications in the *b3galt6*$^{-/-}$ zebrafish might be different from the ones in WT zebrafish.

485   HSPGs and CS/DSPGs are essential macromolecules for the development, signaling and homeostasis

486   of many tissues. It therefore comes as no surprise that defects in linkage region biosynthesis can affect

487   many organs. Endochondral ossification of cartilage (forming chondral bones) for example is a multi-

488   staged process that must be coordinated in space and time. CS/DSPGs and HSPGS, which have key

489 roles in modulating signaling events during vertebrate skeletal development, are expressed in a

490 spatially and temporally highly controlled manner [24], thus regulating the timing of endochondral

491 ossification. Genetic defects disrupting PG synthesis or structure have been shown to disrupt the

492 timing of skeletal development. Two zebrafish models with abnormal PG linkage region biosynthesis,

493 i.e. the *fam20b* and *xylt1*-deficient models, revealed partial decrease in CSPGs, which are

494 predominantly present in cartilage, and accelerated endochondral ossification, showing that CSPGs

495 can negatively regulate skeletogenic timing [24]. On the other hand, a strong reduction in CSPGs and

496 partial decrease in HSPGs was noted in *b3gat3* mutant zebrafish, but this led to a delay in endochondral

497 ossification and short and disorganized cartilaginous structures [39]. Our B3galt6-deficient zebrafish

498 models also show a delay in skeletal development at juvenile stages. At 20 dpf, a delay was noticed in

499 the development of cartilage and mineralized bony elements of the craniofacial structures, the

500 pectoral and caudal fin endoskeleton (Fig. 3B) (Tables S7 and S8), and these abnormalities had

501 progressed in adult zebrafish. The reduced body length, misshapen cranial bones and smaller teeth

502 observed in the head skeleton, and general skeletal dysplasia with kyphosis and scoliosis seen in the

503 vertebral column of *b3galt6*$^{-/-}$ adult zebrafish is reminiscent of the skeletal phenotype observed in

504 human β3GalT6-deficient individuals (Table 2).

505 In addition to skeletal dysplasia, we also observed abnormalities in bone mineralization. Adult mutant

506 zebrafish stained with AR showed the presence of extra intramembranous bone and extra bony

507 elements on the associated elements of the vertebral centra. On the other hand, quantitative μCT

508 analysis of the vertebral column and associated elements revealed a generalized reduction in bone

509 volume and thickness, and a relative increase in TMD after correction for reduced body length of the

510 mutant zebrafish (Fig. 6 and Fig. S13). Although it is not clear so far if the increased fracture risk in

511 spEDS-*B3GALT6* patients can be attributed to a lower bone volume combined with a higher TMD, such

512 hypothesis has been put forward for the brittle bone disorder Osteogenesis Imperfecta (OI) based on

513 observations in both patients and animal models [40, 41]. In the Chihuahua (*col1a1a*$^{chi/+}$) OI zebrafish

514 model the intrafibrillar mineral platelets were shown to be smaller and more densely packed, leading

515 to an increased mineral to matrix ratio, and consequently a reduced elastic modulus-to-hardness ratio,

516 a measure for fracture toughness [41-43]. In addition, in both OI patients and the mouse model *oim,*

517 reduced collagen matrix organization was shown to lead to the formation of extrafibrillar crystals,

518 which are larger compared to intrafibrillar crystals [43]. Eventually, additional minerals stabilize the

519 tissue, but they do so at the cost of increased brittleness of the bone [44]. In accordance, in *b3galt6*$^{-/-}$

520 zebrafish we observed an irregular collagen organization interspersed with large interfibrillar spaces

521 and electron dense spots on ultra-thin sections of skin and bone via TEM. The 'dark spots' observed in

22

522 the vertebral bone could be remnants of extrafibrillar mineral aggregates, contributing to increased

523 mineralization but also increased brittleness of the skeleton.

524 Abnormalities in collagen fibril organization were observed in many mutant zebrafish tissues. Besides

525 vertebral bone, irregular collagen organization was also observed in the intervertebral space,

526 intervertebral ligament, and the dermis. (Fig. 7). This strongly resembles the previously reported

527 abnormal dermal collagen fibril architecture in the skin from a β3GalT6-deficient individual [5]. This

528 could be attributed to abnormalities in GAG chains of small leucine-rich PGs (SLRPs), such as the DSPGs

529 decorin and biglycan, which are known to be of particular importance for regulating collagen fibril

530 organization in connective tissues through their core protein and GAG chains [45]. SLRPs are also

531 thought to influence collagen cross-linking patterns, but the mechanism by which they do so remain

532 largely unknown [45]. Although similar hydroxylation levels were observed at K87 and the C-

533 telopeptide of the type I collagen α1 chain in $b3galt6^{-/-}$ and WT adult zebrafish (Table S9), we cannot

534 rule out that type I collagen cross-linking might still be affected.

535 In view of the observation that human β3GalT6-deficient individuals often present quite severe muscle

536 hypotonia with delayed gross motor development and reduced endurance, we also studied the effect

537 of B3galt6-deficiency on GAG synthesis in muscle, and on muscle function and ultrastructure (Fig. 8).

538 Similar to the other examined tissues, HS and CS/DS GAG concentrations were severely reduced in

539 muscle tissue. It is known that the ECM in skeletal muscle plays an important role in muscle fiber force

540 transmission, maintenance and repair. Numerous PGs, including the HSPGs syndecans 1-4, glypican-1,

541 perlecan and agrin, and CS/DSPGs, such as decorin and biglycan, are present in muscle ECM. Besides

542 their structural role, many of them are known to bind growth factors (e.g. TGFβ). Those growth factors

543 can be stored and released by the negatively charged GAGs. Certain enzymes in the ECM can cleave

544 GAG chains, thereby releasing associated growth factors, allowing their interaction in cell signaling and

545 mechanotransduction [46]. The significant decrease in critical swimming speed (U_{crit}) and endurance

546 observed in the $b3galt6^{-/-}$ zebrafish suggest decreased muscle function (Fig. 8A-B). Further evidence

547 for an intrinsic muscle dysfunction in the $b3galt6^{-/-}$ model comes from semi-thin muscle sections,

548 showing an enlargement of the connective tissue sheet surrounding the muscle fibers (Fig. 8C).

549 Nevertheless, we cannot exclude that the observed skeletal malformations and/or other

550 abnormalities, such as respiratory or neuronal dysfunction, could also influence the outcome of these

551 tests.

552

553

23

Table 2. Clinical features and ultrastructural and biochemical abnormalities observed in spEDS-*B3GALT6* and SEMD-JL1 individuals compared to the *b3galt6*$^{-/-}$ zebrafish model. n.a.: not available. GAG: glycosaminoglycan. The columns 'spEDS-*B3GALT6*' and 'SEMD-JL1' summarize the most important clinical features of all hitherto reported patients for whom this data was available [20, 47].

	Human		Zebrafish
	spEDS-*B3GALT6*	SEMD-JL1	*b3galt6*$^{-/-}$ mutant
General morphology			
Short stature	22/30	11/14	Reduced body length
Craniofacial dysmorphisms (e.g. midfacial hypoplasia, micrognatia)	25/30	12/14	Deformed, small and round head with shorter parietal/occipital region and underdeveloped olfactory region
Dental abnormalities	14/30	n.a.	Smaller teeth
Musculoskeletal involvement			
Bowing of limbs, metaphyseal widening or vertebral body changes	20/30	14/14	Deformities of the fin skeleton
Bone fragility with spontaneous fractures	19/30	0/3	Extra intramembranous bone, lower degree of collagen type I fibril organization and higher TMD after correction for smaller size
Joint contractures (especially hands)	23/30	5/14	Pectoral fins point upwards
Joint hypermobility	26/30	6/14	n.a.
Kyphoscoliosis	23/30	13/14	Kyphosis and scoliosis
Muscle hypotonia	18/30	1/14	Reduced critical swimming speed and endurance
Skin features			
Skin hyperextensibility	19/30	2/14	n.a.
Biochemical findings			
Reduced GAG synthesis	9/9	4/4 (3/4; < HS but > CS/DS)	Reduced GAG production
Ultrastructural findings			
Loosely packed collagen fibrils	1/1	n.a.	Disturbed collagen fibril organization in bone and loosely packed collagen fibrils in the dermis

Taken together, we generated and characterized the first *b3galt6* KO zebrafish models and show that their phenotype largely mimics that of human β3Galt6-deficiency. A strong reduction in HS, CS and DS

561 GAG concentration was observed in *b3galt6*^{-/-} zebrafish. Yet, we did observe a small amount of GAGs

562 being produced with a unique trisaccharide PG linkage region. Furthermore, we showed that a lack of

563 B3galt6 causes disturbances in collagen fibril organization in skin, ligament and bone, with the latter

564 also showing abnormalities in mineralization, and leads to structural and functional abnormalities of

565 the muscle. These KO zebrafish can serve as useful models to further unravel the underlying

566 pathogenic mechanisms of this complex multisystemic disorder and serve as a tool for the

567 development and evaluation of possible therapeutic interventions, such as the stimulation of intrinsic

568 compensational mechanisms for the production of PGs.

569

Material and Methods

570

Zebrafish Maintenance

571

572 Wild-type (AB strain) and *b3galt6* knock-out zebrafish lines were reared and maintained by standard

573 protocols [48]. All animal studies were performed in agreement with EU Directive 2010/63/EU for

574 animals, permit number: ECD 16/18. All zebrafish used in a single experiment were bred at the same

575 density. All efforts were made to minimize pain, distress and discomfort.

Alcian blue and alizarin red staining

576

577 Twenty-day-old larvae (n=10) and five-month-old WT and *b3galt6*^{-/-} (n=5) adult zebrafish were

578 stained as previously described [38]. See Supplementary Information for details.

μCT scanning analysis

579

580 Whole-body μCT scans of four-month-old WT (n=5) and *b3galt6*^{-/-} (n=5) siblings were acquired on a

581 SkyScan 1275 (Bruker, Kontich, Belgium) using the following scan parameters: 0.25 mm aluminum

582 filter, 50 kV, 160 μA, 65 ms integration time, 0.5° rotation step, 721 projections/360°, 5 m 57 s scan

583 duration and 21 μm voxel size. DICOM files of individual zebrafish were segmented in MATLAB using

584 custom FishCuT software and data were analyzed and corrected for standard length in the R statistical

585 environment, as previously described [33].

Histology and transmission electron microscopy

586

587 Zebrafish bone, consisting of the last transitional vertebra and two consecutive caudal vertebrae [49,

588 50], skin, at the lateral line below the dorsal fin, and muscle samples, located dorsolateral underneath

589 the dorsal fin, dissected from five-month-old WT (n=5) and *b3galt6*^{-/-} (n=5) zebrafish, were fixed and

590 embedded in epon following the procedures outlined by Huysseune and Sire [51].

25

591   Swim tunnel experiments

592   Ten WT (five months) and ten *b3galt6*^{-/-} zebrafish (eight months), were selected based on their similar

593   (not significantly different) length and weight. The critical swimming speed (U_{crit}) was measured in a

594   swim tunnel for both WT and *b3galt6*^{-/-} zebrafish as previously described [52]. Furthermore, the

595   endurance of each zebrafish was tested by means of an effort test in the swim tunnel. Each zebrafish

596   had a three minute warm-up and after the third minute, the speed increased until 37 cm/s for

597   maximum 7 minutes. When the zebrafish was not able to swim anymore, the test was stopped.

598   Collagen crosslinking analysis

599   The collagen crosslinking was analyzed in the dissected vertebral column (excluding Weberian

600   apparatus and urostyle) from five-month-old wild-type (n=5) and *b3galt6*^{-/-} (n=5) siblings as described

601   before in Gistelinck *et al.* [40].

602   Disaccharide composition analysis of CS, DS, and HS chains

603   The level of total disaccharides from CS, DS, and HS in bone, muscle and skin tissues from nine-month-

604   old zebrafish (n=5) were determined as described previously [53, 54].

605   Glycopeptide preparation and analysis

606   **LC-MS/MS sample preparation -** CS- and HS-glycopeptides were purified from six-month-old WT (n=3)

607   and *b3galt6*^{-/-} (n=3) zebrafish using a combination of extraction, trypsin digestion and anion exchange

608   chromatography, slightly modified (see Supplementary Information) from previously described

609   protocols [27, 55].

610   **LC-MS/MS analysis -** The samples were analyzed on an Orbitrap Fusion mass spectrometer coupled to

611   an Easy-nLC 1200 liquid chromatography system (Thermo Fisher Scientific., Waltham, MA) (see

612   Supplementary Information). Nanospray Flex ion source was operated in positive ionization mode and

613   three separate higher-energy collision-induced dissociation (HCD) MS/MS spectra were recorded for

614   each precursor ion [27, 55].

615   **LC-MS/MS data analysis -** The glycopeptide files were analyzed using both manual interpretation and

616   automated Mascot searches for GAG-glycopeptides. The files were manually interpreted using the

617   Xcalibur software (Thermo Fisher Scientific). Database searches were performed against *Danio rerio* in

618   the UniProtKB/Swiss-Prot database and NCBI using Mascot Distiller (version 2.6.1.0, Matrix Science,

619   London, U.K) and an in-house Mascot server (version 2.5.1). Glycan structures with very small mass

620   differences were manually evaluated at the MS2-level.

26

621   GlcAT-I assay

622   GlcA-transferase assay was carried out by the methodology as previously described [12, 56, 57], with
623   slight modifications.

624   Detailed information regarding the procedures used is provided in SI Appendix, Supplementary
625   Material and Methods.

626

Conflict of interest statement

628   The authors declare no competing interests. Author Phil L. Salmon was employed by the company
629   Bruker MicroCT. The remaining authors declare that the research was conducted in the absence of
630   any commercial or financial relationships that could be construed as a potential conflict of interest.

631

Acknowledgements

640

Funding

651

References

[1] K. Prydz, K.T. Dalen, Synthesis and sorting of proteoglycans - Commentary, J Cell Sci 113(2) (2000) 193-205.

[2] J.R. Couchman, C.A. Pataki, An introduction to proteoglycans and their localization, J Histochem Cytochem 60(12) (2012) 885-97.

[3] U. Lindahl, J. Couchman, K. Kimata, J.D. Esko, Proteoglycans and Sulfated Glycosaminoglycans, in: rd, A. Varki, R.D. Cummings, J.D. Esko, P. Stanley, G.W. Hart, M. Aebi, A.G. Darvill, T. Kinoshita, N.H. Packer, J.H. Prestegard, R.L. Schnaar, P.H. Seeberger (Eds.), Essentials of Glycobiology, Cold Spring Harbor (NY), 2015, pp. 207-221.

[4] S.B. Selleck, Proteoglycans and pattern formation: sugar biochemistry meets developmental genetics, Trends Genet 16(5) (2000) 206-12.

[5] F. Malfait, A. Kariminejad, T. Van Damme, C. Gauche, D. Syx, F. Merhi-Soussi, S. Gulberti, S. Symoens, S. Vanhauwaert, A. Willaert, B. Bozorgmehr, M.H. Kariminejad, N. Ebrahimiadib, I. Hausser, A. Huysseune, S. Fournel-Gigleux, A. De Paepe, Defective Initiation of Glycosaminoglycan Synthesis due to B3GALT6 Mutations Causes a Pleiotropic Ehlers-Danlos-Syndrome-like Connective Tissue Disorder, Am J Hum Genet 92(6) (2013) 935-945.

[6] K. Sugahara, T. Mikami, T. Uyama, S. Mizuguchi, K. Nomura, H. Kitagawa, Recent advances in the structural biology of chondroitin sulfate and dermatan sulfate, Curr Opin Struct Biol 13(5) (2003) 612-20.

[7] M. Kusche-Gullberg, L. Kjellen, Sulfotransferases in glycosaminoglycan biosynthesis, Curr Opin Struct Biol 13(5) (2003) 605-11.

[8] C. Bui, M. Ouzzine, I. Talhaoui, S. Sharp, K. Prydz, M.W. Coughtrie, S. Fournel-Gigleux, Epigenetics: methylation-associated repression of heparan sulfate 3-O-sulfotransferase gene expression contributes to the invasive phenotype of H-EMC-SS chondrosarcoma cells, FASEB J 24(2) (2010) 436-50.

[9] C. Gotting, J. Kuhn, R. Zahn, T. Brinkmann, K. Kleesiek, Molecular cloning and expression of human UDP-d-Xylose:proteoglycan core protein beta-d-xylosyltransferase and its first isoform XT-II, J Mol Biol 304(4) (2000) 517-28.

[10] R. Almeida, S.B. Levery, U. Mandel, H. Kresse, T. Schwientek, E.P. Bennett, H. Clausen, Cloning and expression of a proteoglycan UDP-galactose:beta-xylose beta1,4-galactosyltransferase I. A seventh member of the human beta4-galactosyltransferase gene family, J Biol Chem 274(37) (1999) 26165-71.

28

684 [11] X. Bai, D. Zhou, J.R. Brown, B.E. Crawford, T. Hennet, J.D. Esko, Biosynthesis of the linkage region

685 of glycosaminoglycans: cloning and activity of galactosyltransferase II, the sixth member of the beta

686 1,3-galactosyltransferase family (beta 3GalT6), J Biol Chem 276(51) (2001) 48189-95.

687 [12] H. Kitagawa, Y. Tone, J. Tamura, K.W. Neumann, T. Ogawa, S. Oka, T. Kawasaki, K. Sugahara,

688 Molecular cloning and expression of glucuronyltransferase I involved in the biosynthesis of the

689 glycosaminoglycan-protein linkage region of proteoglycans, J Biol Chem 273(12) (1998) 6615-8.

690 [13] J. Wen, J. Xiao, M. Rahdar, B.P. Choudhury, J. Cui, G.S. Taylor, J.D. Esko, J.E. Dixon, Xylose

691 phosphorylation functions as a molecular switch to regulate proteoglycan biosynthesis, Proc Natl

692 Acad Sci U S A 111(44) (2014) 15723-8.

693 [14] K.L. Jones, U. Schwarze, M.P. Adam, P.H. Byers, H.C. Mefford, A homozygous B3GAT3 mutation

694 causes a severe syndrome with multiple fractures, expanding the phenotype of linkeropathy

695 syndromes, Am J Med Genet A 167A(11) (2015) 2691-6.

696 [15] M.H. Guo, J. Stoler, J. Lui, O. Nilsson, D.W. Bianchi, J.N. Hirschhorn, A. Dauber, Redefining the

697 progeroid form of Ehlers-Danlos syndrome: report of the fourth patient with B4GALT7 deficiency and

698 review of the literature, Am J Med Genet A 161A(10) (2013) 2519-27.

699 [16] M. Nakajima, S. Mizumoto, N. Miyake, R. Kogawa, A. Iida, H. Ito, H. Kitoh, A. Hirayama, H.

700 Mitsubuchi, O. Miyazaki, R. Kosaki, R. Horikawa, A. Lai, R. Mendoza-Londono, L. Dupuis, D. Chitayat,

701 A. Howard, G.F. Leal, D. Cavalcanti, Y. Tsurusaki, H. Saitsu, S. Watanabe, E. Lausch, S. Unger, L.

702 Bonafe, H. Ohashi, A. Superti-Furga, N. Matsumoto, K. Sugahara, G. Nishimura, S. Ikegawa, Mutations

703 in B3GALT6, which encodes a glycosaminoglycan linker region enzyme, cause a spectrum of skeletal

704 and connective tissue disorders, Am J Hum Genet 92(6) (2013) 927-34.

705 [17] F. Malfait, A. Kariminejad, T. Van Damme, C. Gauche, D. Syx, F. Merhi-Soussi, S. Gulberti, S.

706 Symoens, S. Vanhauwaert, A. Willaert, B. Bozorgmehr, M.H. Kariminejad, N. Ebrahimiadib, I. Hausser,

707 A. Huysseune, S. Fournel-Gigleux, A. De Paepe, Defective initiation of glycosaminoglycan synthesis

708 due to B3GALT6 mutations causes a pleiotropic Ehlers-Danlos-syndrome-like connective tissue

709 disorder, Am J Hum Genet 92(6) (2013) 935-45.

710 [18] F. Malfait, C. Francomano, P. Byers, J. Belmont, B. Berglund, J. Black, L. Bloom, J.M. Bowen, A.F.

711 Brady, N.P. Burrows, M. Castori, H. Cohen, M. Colombi, S. Demirdas, J. De Backer, A. De Paepe, S.

712 Fournel-Gigleux, M. Frank, N. Ghali, C. Giunta, R. Grahame, A. Hakim, X. Jeunemaitre, D. Johnson, B.

713 Juul-Kristensen, I. Kapferer-Seebacher, H. Kazkaz, T. Kosho, M.E. Lavallee, H. Levy, R. Mendoza-

714 Londono, M. Pepin, F.M. Pope, E. Reinstein, L. Robert, M. Rohrbach, L. Sanders, G.J. Sobey, T. Van

715 Damme, A. Vandersteen, C. van Mourik, N. Voermans, N. Wheeldon, J. Zschocke, B. Tinkle, The 2017

716 international classification of the Ehlers-Danlos syndromes, Am J Med Genet C Semin Med Genet

717 175(1) (2017) 8-26.

718 [19] M. Ritelli, N. Chiarelli, N. Zoppi, C. Dordoni, S. Quinzani, M. Traversa, M. Venturini, P. Calzavara-
719 Pinton, M. Colombi, Insights in the etiopathology of galactosyltransferase II (GalT-II) deficiency from
720 transcriptome-wide expression profiling of skin fibroblasts of two sisters with compound
721 heterozygosity for two novel B3GALT6 mutations, Mol Genet Metab Rep 2 (2015) 1-15.

722 [20] T. Van Damme, X. Pang, B. Guillemyn, S. Gulberti, D. Syx, R. De Rycke, O. Kaye, C.E.M. de Die-
723 Smulders, R. Pfundt, A. Kariminejad, S. Nampoothiri, G. Pierquin, S. Bulk, A.A. Larson, K.C. Chatfield,
724 M. Simon, A. Legrand, M. Gerard, S. Symoens, S. Fournel-Gigleux, F. Malfait, Biallelic B3GALT6
725 mutations cause spondylodysplastic Ehlers-Danlos syndrome, Hum Mol Genet 27(20) (2018) 3475-
726 3487.

727 [21] C. Santoriello, L.I. Zon, Hooked! Modeling human disease in zebrafish, J Clin Invest 122(7) (2012)
728 2337-43.

729 [22] K. Dooley, L.I. Zon, Zebrafish: a model system for the study of human disease, Curr Opin Genet
730 Dev 10(3) (2000) 252-6.

731 [23] B.F. Eames, A. Singer, G.A. Smith, Z.A. Wood, Y.L. Yan, X. He, S.J. Polizzi, J.M. Catchen, A.
732 Rodriguez-Mari, T. Linbo, D.W. Raible, J.H. Postlethwait, UDP xylose synthase 1 is required for
733 morphogenesis and histogenesis of the craniofacial skeleton, Dev Biol 341(2) (2010) 400-15.

734 [24] B.F. Eames, Y.L. Yan, M.E. Swartz, D.S. Levic, E.W. Knapik, J.H. Postlethwait, C.B. Kimmel,
735 Mutations in fam20b and xylt1 reveal that cartilage matrix controls timing of endochondral
736 ossification by inhibiting chondrocyte maturation, PLoS Genet 7(8) (2011) e1002246.

737 [25] A. Amsterdam, R.M. Nissen, Z. Sun, E.C. Swindell, S. Farrington, N. Hopkins, Identification of 315
738 genes essential for early zebrafish development, Proc Natl Acad Sci U S A 101(35) (2004) 12792-7.

739 [26] R.M. Nissen, A. Amsterdam, N. Hopkins, A zebrafish screen for craniofacial mutants identifies
740 wdr68 as a highly conserved gene required for endothelin-1 expression, BMC Dev Biol 6 (2006) 28.

741 [27] F. Noborn, A. Gomez Toledo, C. Sihlbom, J. Lengqvist, E. Fries, L. Kjellen, J. Nilsson, G. Larson,
742 Identification of chondroitin sulfate linkage region glycopeptides reveals prohormones as a novel
743 class of proteoglycans, Mol Cell Proteomics 14(1) (2015) 41-9.

744 [28] A. Persson, J. Nilsson, E. Vorontsov, F. Noborn, G. Larson, Identification of a non-canonical
745 chondroitin sulfate linkage region trisaccharide, Glycobiology 29(5) (2019) 366-371.

746 [29] R.D.M. Nash, A.H. Valencia, A.J. Geffen, The origin of Fulton's condition factor - Setting the
747 record straight, Fisheries 31(5) (2006) 236-238.

748 [30] G. Arratia, H.P. Schultze, Reevaluation of the caudal skeleton of certain actinopterygian fishes:
749 III. Salmonidae. Homologization of caudal skeletal structures, J Morphol 214(2) (1992) 187-249.

750 [31] S.K. McMenamin, M.N. Chandless, D.M. Parichy, Working with zebrafish at postembryonic
751 stages, Methods Cell Biol 134 (2016) 587-607.

752   [32] D.M. Parichy, M.R. Elizondo, M.G. Mills, T.N. Gordon, R.E. Engeszer, Normal table of

753   postembryonic zebrafish development: staging by externally visible anatomy of the living fish, Dev

754   Dyn 238(12) (2009) 2975-3015.

755   [33] M. Hur, C.A. Gistelinck, P. Huber, J. Lee, M.H. Thompson, A.T. Monstad-Rios, C.J. Watson, S.K.

756   McMenamin, A. Willaert, D.M. Parichy, P. Coucke, R.Y. Kwon, MicroCT-based phenomics in the

757   zebrafish skeleton reveals virtues of deep phenotyping in a distributed organ system, Elife 6 (2017).

758   [34] C. Gistelinck, R. Gioia, A. Gagliardi, F. Tonelli, L. Marchese, L. Bianchi, C. Landi, L. Bini, A.

759   Huysseune, P.E. Witten, A. Staes, K. Gevaert, N. De Rocker, B. Menten, F. Malfait, S. Leikin, S. Carra,

760   R. Tenni, A. Rossi, A. De Paepe, P. Coucke, A. Willaert, A. Forlino, Zebrafish Collagen Type I: Molecular

761   and Biochemical Characterization of the Major Structural Protein in Bone and Skin, Sci Rep 6 (2016)

762   21540.

763   [35] I. Plaut, Effects of fin size on swimming performance, swimming behaviour and routine activity

764   of zebrafish Danio rerio, J Exp Biol 203(Pt 4) (2000) 813-20.

765   [36] N. Wittkopp, E. Huntzinger, C. Weiler, J. Sauliere, S. Schmidt, M. Sonawane, E. Izaurralde,

766   Nonsense-mediated mRNA decay effectors are essential for zebrafish embryonic development and

767   survival, Mol Cell Biol 29(13) (2009) 3517-28.

768   [37] Y.H. Chen, Y. Narimatsu, T.M. Clausen, C. Gomes, R. Karlsson, C. Steentoft, C.B. Spliid, T.

769   Gustavsson, A. Salanti, A. Persson, A. Malmstrom, D. Willen, U. Ellervik, E.P. Bennett, Y. Mao, H.

770   Clausen, Z. Yang, The GAGOme: a cell-based library of displayed glycosaminoglycans, Nat Methods

771   15(11) (2018) 881-888.

772   [38] S. Delbaere, T. Van Damme, D. Syx, S. Symoens, P. Coucke, A. Willaert, F. Malfait, Hypomorphic

773   zebrafish models mimic the musculoskeletal phenotype of beta4GalT7-deficient Ehlers-Danlos

774   syndrome, Matrix Biol 89 (2020) 59-75.

775   [39] K. Holmborn, J. Habicher, Z. Kasza, A.S. Eriksson, B. Filipek-Gorniok, S. Gopal, J.R. Couchman, P.E.

776   Ahlberg, M. Wiweger, D. Spillmann, J. Kreuger, J. Ledin, On the roles and regulation of chondroitin

777   sulfate and heparan sulfate in zebrafish pharyngeal cartilage morphogenesis, J Biol Chem 287(40)

778   (2012) 33905-16.

779   [40] C. Gistelinck, P.E. Witten, A. Huysseune, S. Symoens, F. Malfait, D. Larionova, P. Simoens, M.

780   Dierick, L. Van Hoorebeke, A. De Paepe, R.Y. Kwon, M. Weis, D.R. Eyre, A. Willaert, P.J. Coucke, Loss

781   of Type I Collagen Telopeptide Lysyl Hydroxylation Causes Musculoskeletal Abnormalities in a

782   Zebrafish Model of Bruck Syndrome, J Bone Miner Res 31(11) (2016) 1930-1942.

783   [41] I.A.K. Fiedler, F.N. Schmidt, E.M. Wolfel, C. Plumeyer, P. Milovanovic, R. Gioia, F. Tonelli, H.A.

784   Bale, K. Jahn, R. Besio, A. Forlino, B. Busse, Severely Impaired Bone Material Quality in Chihuahua

785 Zebrafish Resembles Classical Dominant Human Osteogenesis Imperfecta, Journal of Bone and

786 Mineral Research 33(8) (2018) 1489-1499.

787 [42] N. Bishop, Bone Material Properties in Osteogenesis Imperfecta, J Bone Miner Res 31(4) (2016)

788 699-708.

789 [43] S. Viguet-Carrin, P. Garnero, P.D. Delmas, The role of collagen in bone strength, Osteoporos Int

790 17(3) (2006) 319-36.

791 [44] B. Grabner, W.J. Landis, P. Roschger, S. Rinnerthaler, H. Peterlik, K. Klaushofer, P. Fratzl, Age-

792 and genotype-dependence of bone material properties in the osteogenesis imperfecta murine model

793 (oim), Bone 29(5) (2001) 453-7.

794 [45] S. Kalamajski, A. Oldberg, The role of small leucine-rich proteoglycans in collagen fibrillogenesis,

795 Matrix Biol 29(4) (2010) 248-53.

796 [46] A.R. Gillies, R.L. Lieber, Structure and function of the skeletal muscle extracellular matrix, Muscle

797 Nerve 44(3) (2011) 318-31.

798 [47] S.G. Caraffi, I. Maini, I. Ivanovski, M. Pollazzon, S. Giangiobbe, M. Valli, A. Rossi, S. Sassi, S.

799 Faccioli, M.D. Rocco, C. Magnani, B. Campos-Xavier, S. Unger, A. Superti-Furga, L. Garavelli, Severe

800 Peripheral Joint Laxity is a Distinctive Clinical Feature of Spondylodysplastic-Ehlers-Danlos Syndrome

801 (EDS)-B4GALT7 and Spondylodysplastic-EDS-B3GALT6, Genes (Basel) 10(10) (2019).

802 [48] C. Gistelinck, R.Y. Kwon, F. Malfait, S. Symoens, M.P. Harris, K. Henke, M.B. Hawkins, S. Fisher, P.

803 Sips, B. Guillemyn, J.W. Bek, P. Vermassen, H. De Saffel, P.E. Witten, M. Weis, A. De Paepe, D.R. Eyre,

804 A. Willaert, P.J. Coucke, Zebrafish type I collagen mutants faithfully recapitulate human type I

805 collagenopathies, Proc Natl Acad Sci U S A 115(34) (2018) E8037-E8046.

806 [49] N.C. Bird, P.M. Mabee, Developmental morphology of the axial skeleton of the zebrafish, Danio

807 rerio (Ostariophysi: Cyprinidae), Dev Dyn 228(3) (2003) 337-57.

808 [50] E.M. Morin-Kensicki, E. Melancon, J.S. Eisen, Segmental relationship between somites and

809 vertebral column in zebrafish, Development 129(16) (2002) 3851-3860.

810 [51] A. Huysseune, J.Y. Sire, Bone and cartilage resorption in relation to tooth development in the

811 anterior part of the mandible in cichlid fish: a light and TEM study, Anat Rec 234(1) (1992) 1-14.

812 [52] J.R. Brett, The Respiratory Metabolism and Swimming Performance of Young Sockeye Salmon, J

813 Fish Res Board Can 21(5) (1964) 1183-1226.

814 [53] S. Mizumoto, T. Mikami, D. Yasunaga, N. Kobayashi, H. Yamauchi, A. Miyake, N. Itoh, H.

815 Kitagawa, K. Sugahara, Chondroitin 4-O-sulfotransferase-1 is required for somitic muscle

816 development and motor axon guidance in zebrafish, Biochem J 419(2) (2009) 387-99.

817 [54] S. Mizumoto, K. Sugahara, Glycosaminoglycan chain analysis and characterization

818 (glycosylation/epimerization), Methods Mol Biol 836 (2012) 99-115.

819   [55] F. Noborn, A. Gomez Toledo, A. Green, W. Nasir, C. Sihlbom, J. Nilsson, G. Larson, Site-specific

820   identification of heparan and chondroitin sulfate glycosaminoglycans in hybrid proteoglycans, Sci Rep

821   6 (2016) 34537.

822   [56] S. Baasanjav, L. Al-Gazali, T. Hashiguchi, S. Mizumoto, B. Fischer, D. Horn, D. Seelow, B.R. Ali, S.A.

823   Aziz, R. Langer, A.A. Saleh, C. Becker, G. Nurnberg, V. Cantagrel, J.G. Gleeson, D. Gomez, J.B. Michel,

824   S. Stricker, T.H. Lindner, P. Nurnberg, K. Sugahara, S. Mundlos, K. Hoffmann, Faulty initiation of

825   proteoglycan synthesis causes cardiac and joint defects, Am J Hum Genet 89(1) (2011) 15-27.

826   [57] F. Job, S. Mizumoto, L. Smith, N. Couser, A. Brazil, H. Saal, M. Patterson, M.I. Gibson, S. Soden, N.

827   Miller, I. Thiffault, C. Saunders, S. Yamada, K. Hoffmann, K. Sugahara, E. Farrow, Functional validation

828   of novel compound heterozygous variants in B3GAT3 resulting in severe osteopenia and fractures:

829   expanding the disease phenotype, BMC Med Genet 17(1) (2016) 86.

830   [58] S. Delbaere, A. De Clercq, S. Mizumoto, F. Noborn, J.W. Bek, L. Alluyn, C. Gistelinck, D. Syx, P.L.

831   Salmon, P.J. Coucke, G. Larson, S. Yamada, A. Willaert, F. Malfait, *b3galt6* knock-out zebrafish

832   recapitulate β3GalT6-deficiency disorders in human and reveal a trisaccharide proteoglycan linkage

833   region, bioRxiv (2020) 2020.06.22.165316.

834